A method for early-stage design current loads determination on drill-ships

Mauro, Francesco; Valentina, Enrico Della; Ferrari, Victor; Begovic, Ermina

DOI
10.1016/j.oceaneng.2023.115716

Publication date
2023

Document Version
Final published version

Published in
Ocean Engineering

Ocean Engineering 287 (2023) 115716

Contents lists available at ScienceDirect

Ocean Engineering

journal homepage: www.elsevier.com/locate/oceaneng

A method for early-stage design current loads determination on drill-ships

Francesco Mauro [a,b,*], Enrico Della Valentina [c], Victor Ferrari [c], Ermina Begovic [d]

[a] Department of Maritime and Transport Technology, Faculty of Mechanical. Maritime and Materials Engineering, Delft University of Technology, Leegwaterstraat 17, 2628 CA Delft, The Netherlands

[b] Sharjah Maritime Academy, 180018, Khorfakkan, Sharjah, United Arab Emirates

[c] Maritime Research Institute of the Netherlands - MARIN, Wageningen, The Netherlands

[d] Department of Industrial Engineering, University of Naples Federico II, Naples, 80125, Italy

ARTICLE INFO

Keywords:
Current loads
CFD
Drill-ships
Dynamic positioning
Hull forms

ABSTRACT

The increasing demand for offshore operations in deep water implies the necessity to predict station-keeping ability of offshore vessels since the early stages of design. To this end, besides developing sufficiently fast and accurate methodologies for the equilibrium resolution of the forces acting on the ship, it is of utmost importance to estimate, in a reliable way, the external forces acting on the vessel. This work focuses on the current loads, aiming at developing a model for fast current load prediction based on high-fidelity Computational Fluid Dynamics (CFD) computations. Selecting the drill-ships as reference vessel-type for the study, starting from the actual fleet operating worldwide, a systematic series of hulls has been generated varying the main hull-form parameters inside the database, according to a Box-Behnken scheme. CFD calculations based on RANS equations have been performed on the whole ship set, for a set of incidence angle varying from 0 to 180 degrees considering the hull symmetric. As numerical analyses are not suitable for fast calculations the results on the systematic series have been used as input for developing a surrogate model based on Multiple Linear Regressions (MLR). The method allows for scaling the results as a function of the Reynolds number, allowing for general and flexible applicability among different vessel dimensions. The results obtained with the developed model are compared with the conventional current loads estimation methods, and the obtained results are compared on the capability plot, highlighting the higher reliability of the proposed model for early-stage predictions.

1. Introduction

The determination of the station-keeping ability is an issue that is now mandatory for a large number of offshore vessels, as the continuous transition of offshore operations to deeper water requires the use of onboard actuators for stationing in operative areas (Nabergoj, 2011). Such an issue is not restricted to offshore vessels but starts to be significant also for leisure crafts stationing in environmentally protected areas (Mauro et al., 2020, 2021). Furthermore, the same issues associated with the dynamic positioning of an offshore ship are similar to crabbing and station-keeping of vessels like cruises and ferries during harbour manoeuvers (Ferrari et al., 2019).

Notwithstanding the above, the present paper focuses on station-keeping for offshore vessels, selecting as reference ship type the drill-ships. Station-keeping problems deal with the ability of a vessel to autonomously counteract the external loads acting on the ship, which are mainly composed of environmental loads of wind, waves and current. The station-keeping ability can be assessed through time-domain simulations (Smogeli et al., 2013; Martelli et al., 2022) or, especially in an early design stage, by using quasi-static calculations (Wang et al., 2018). This paper considers the input necessary to evaluate the vessel's station-keeping ability by employing quasi-static methods, targeting the early-stage design. In such a case, the problem reduces to finding the equilibrium of forces and moments between the external loads and the thrust delivered by onboard actuators. Therefore, determining environmental loads is a focal point for early-stage design station-keeping predictions.

Among the environmental loads acting on a ship, generally, the current is less incisive in the total amount of external forces. However, it remains still a considerable load, especially for special operations, like those close to estuaries, where it could represent the preeminent load. Therefore, the preliminary estimation of current loads is necessary, not only for offshore vessels but also for other kinds of operations like crabbing for passenger ships.

* Corresponding author at: Department of Maritime and Transport Technology, Faculty of Mechanical. Maritime and Materials Engineering, Delft University of Technology, Leegwaterstraat 17, 2628 CA Delft, The Netherlands.

E-mail addresses: F.Mauro@tudelft.nl (F. Mauro), E.Valentina@marin.nl (E.D. Valentina), V.Ferrari@marin.nl (V. Ferrari), E.begovic@unina.it (E. Begovic).

https://doi.org/10.1016/j.oceaneng.2023.115716
Received 8 May 2023; Received in revised form 9 August 2023; Accepted 24 August 2023
Available online 4 September 2023

The present study focuses on current loads for offshore applications, where general empirical methods for current loads estimation are present (API, 1984; OCIMF, 1994; DNV-GL, 2018), but fast higher fidelity models, applicable in the early design stage, are missing (Yuck et al., 2005; Aydın et al., 2022). The most reliable way to determine current loads is, for sure, using model tests, but the costs and design accuracy level required to perform them are too high for an early design stage (Ottens et al., 2009). Besides model tests, a promising technique is the viscous flow CFD calculations (Kim et al., 2009; Vaz et al., 2009; Koop et al., 2013). In any case, this approach requires a high computational time and also a high level skilled designers to obtain reliable results from calculations (Koop, 2020). It is then convenient to provide fast, simplified surrogate models obtained by databases of higher fidelity calculations. To this end, the present work considers the development of a surrogate model derived from viscous flow CFD calculations.

The application of viscous flow calculation for current loads allows simplifications of the numerical models involved in the calculations, especially when no significant appendages are fitted to the geometrical model. In fact, due to the low speed of the current, there is no need to simulate the water free surface, choosing a faster double-body calculation.

Such a matter allows for obtaining the current loads in a reasonable calculation time. Then, applying such techniques for developing a database of forces is reliable, but calculations still require a reasonable time. As no open literature reference is present for drill-ship hulls, a systematic series of hull forms has been developed starting from a parent hull, representative of a standard modern drill-ship hull. The systematic series comprises variations on L/B, B/T ratios and block coefficient C_B, keeping other parameters like the longitudinal centre of buoyancy x_B constant. The hull variations have been determined with the design of experiments (DOE) technique, applying the Box-Behnken method. Afterwards, model-scale CFD calculations have performed on the resulting 15 hull forms, considering a model of 8 metres, using calculation set-up and domain discretisation validated with reference model tests on a VLCC (Very Large Crude Carrier) hull for small headings, ensuring mesh independence for large ones. Calculations include a range of headings from 0 to 180 degrees, considering, for this first analysis, no relevant appendages fitted on the hull.

The results obtained from the computations represent the viscous resistance acting on the hull at several headings. Therefore a different and original approach to calculate the current coefficient is proposed. The model-scale coefficient allows evaluating a current form factor employing a standard friction line like the ITTC 57. Afterwards, the full-scale coefficient can be obtained by multiplying the current form factor by the full-scale friction line coefficient. Such an approach allows more flexibility in evaluating current loads for vessels with different lengths. Adopting response surface methodology (RSM), multiple linear regressions have been carried out on the current form factor, generating a flexible surrogate model for current load evaluation.

As final result, the newly developed current coefficient model is compared with the conventional methods employed for current loads estimation in the preliminary station-keeping analyses on a reference drill-ship. Firstly, the current forces are directly compared, underlining the differences between the presented methodologies. Then, the effect of the multiple loads' sources is visualised in the capability plots, highlighting the differences in the DP capabilities of the reference vessel. The results highlight large differences between the methods, underlining the importance of using higher fidelity models, like the one proposed here, for the numerical current load predictions.

2. Current loads in station-keeping

Current load estimation is a relevant issue for ships dealing with mooring, station-keeping or crabbing problems. Even though the mentioned application fields are different, the main issue is to keep the vessel in a determined position under the action of external loads acting on the ship or determine the maximum environmental forces the mooring/thruster system can counteract.

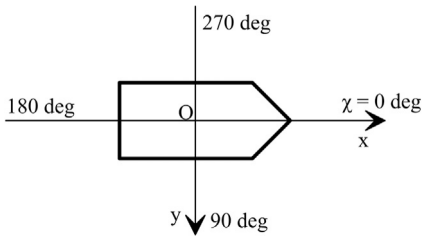

Fig. 1. Reference system for station-keeping calculations.

Regardless of the type of problem to be faced, there are two main possibilities to evaluate the capability of the onboard systems: time-domain simulations (Smogeli et al., 2013; Mauro and Gaudiano, 2018; Martelli et al., 2022) or quasi-static calculations (Aalberts et al., 1995; Wang et al., 2018).

The first method is more time-consuming and requires the modelling and knowledge of systems and parameters rarely available during the early design stage. It is, therefore, advisable to adopt such an approach during a more advanced design stage. For early-design calculation, the quasi-static predictions are the most convenient and flexible option to check the capability of the system under analysis, concurrently evaluating multiple alternatives (Mauro and Nabergoj, 2019).

The quasi-static method consists in solving the equilibrium of forces/moments acting on the vessel on the horizontal plane, taking into account the dynamic effects through allowances on the external forces. Considering a body-fixed reference system as reported in Fig. 1, the 3 degrees of freedom equations, in compact form, to solve are:

$$\boldsymbol{f_{ext}} = \boldsymbol{A}(\boldsymbol{\alpha})\, \boldsymbol{f_a} \tag{1}$$

where $\boldsymbol{f_a} = \left[f_{a_1}, \ldots, f_{a_{N_a}}\right]^T$ is the vector of forces given by the N_a onboard actuators, and $\boldsymbol{f_{ext}} = \left[F_{x_{ext}}, F_{y_{ext}}, M_{z_{ext}}\right]^T$ is the vector of external forces acting on the vessel. $\boldsymbol{A} \in \mathbb{R}^{3\times N_a}$ is a vessel-specific matrix depending on the actuators type, and contains the locations and thrust orientation vector $\boldsymbol{\alpha} = \left[\alpha_1, \ldots, \alpha_{N_a}\right]^T$. For the typical actuators of a DP system, each one of the N_a column vectors $\boldsymbol{a}_i \in \mathbb{R}^3$ composing matrix $\boldsymbol{A}$ are as follows:

$$\boldsymbol{a}_i = \begin{cases} \left[1, 0, -y_{a_i}\right]^T & \text{main propellers} \\ \left[0, 1, x_{a_i}\right]^T & \text{fixed tunnel thrusters or rudders} \\ \left[\cos\alpha_i, \sin\alpha_i, x_{a_i}\sin\alpha_i - y_{a_i}\cos\alpha_i\right]^T & \text{azimuth thr.} \end{cases}$$

where x_{a_i} and y_{a_i} are the longitudinal and lateral positions of the actuators, respectively. Generally, offshore ships or vessels equipped with a DP system have a number of actuators N_a such that the total number of unknowns is higher than the rank of system (1), which, consequently, admits infinite solutions. For such a reason, the system needs to be solved using a specific thrust allocation algorithm, usually employing simple or advanced optimisation techniques widely discussed in the literature. Here, the focus is on station-keeping as the reference vessel chosen for the study (i.e. a drill-ship) is mainly oriented to DP operations. Notwithstanding the above, the considerations and further model proposals remain valid also for other purposes.

The principal interest for this study is the left term of system (1), means the external forces vector $\boldsymbol{f_{ext}}$. The external forces vector has generally the following breakdown:

$$\boldsymbol{f_{ext}} = \boldsymbol{f_{env}} + \boldsymbol{f_{op}} \tag{2}$$

where $\boldsymbol{f}_{env}$ are the environmental forces, and $\boldsymbol{f}_{op}$ are additional forces specific for particular operations a vessel performs while operating the DP system (Ardavanis et al., 2022). Most of the times, the $\boldsymbol{f}_{op}$ vector is not known in an early design stage; thus, the external forces vector reduces to the environmental forces as a function of the different environmental loads acting on the ship:

$$\boldsymbol{f}_{env} = \left(\boldsymbol{f}_{\boldsymbol{W}} + \boldsymbol{f}_{\boldsymbol{w}} + \boldsymbol{f}_{\boldsymbol{c}}\right) CA_{dyn}, \tag{3}$$

where $\boldsymbol{f}_{\boldsymbol{W}} = \left[F_{x_W}.F_{y_W}, M_{z_W}\right]^T$ are the wind loads, $\boldsymbol{f}_{\boldsymbol{w}} = \left[F_{x_w}.F_{y_w}, M_{z_w}\right]^T$ are the wave loads and $\boldsymbol{f}_{\boldsymbol{c}} = \left[F_{x_c}.F_{y_c}, M_{z_c}\right]^T$ are the current loads. CA_{dyn} is an allowance coefficient employed as an expedient to include dynamic effects in quasi-static DP predictions. Such a coefficient may be empirical, suggested by Classification guidelines or derived from time-domain simulations on similar vessels.

With the focus of this study on the current loads, the present paper does not discuss the effect of wind and waves, even though they are most of the time the dominant part of the environmental loads. Nonetheless, current may be dominant for several special conditions, like operation close to an estuary or in the presence of particularly strong local streams. Therefore, the estimation of the current loads is relevant for the early design stage.

There are several possibilities to determine the current loads, corresponding to different fidelity levels. The highest fidelity method is the model test; however, the execution of such tests is expensive and requires the definition of the hull and all relevant appendages. As the required information is not at our disposal in early design stage, model tests are an option in advanced design stages. In the second instance, viscous flow CFD calculations are a promising technique for current load estimation, but they still require data and calculation times not suitable for the early design stage. For the initial phases of a design, it is preferable to use simplified methods suggested by Classification Societies or general guidelines, requiring few inputs to estimate the loads. Such methods are briefly presented in the next section and in Appendix A, together with the development of a new and original estimation method based on surrogate models obtained from higher fidelity CFD computations.

2.1. Standard current loads determination for early-stage design

In an early design stage, it is usual to adopt simple methods mainly based on Classification Societies indications; or, as a second choice, using coefficients from model-scale measurements on similar vessels. Since the second option is something not available in the literature, Appendix A briefly describes the most commonly used methods from regulations. To avoid misinterpretation between different methods that use alternative reference systems, conventions and units; here, a single form is used for determining non-dimensional coefficients of current loads, employing the reference system previously described for DP calculations in Fig. 1. By employing the ship wetted surface S, the non-dimensional coefficients assume the following form:

$$C_{x_c}\left(\chi_c\right) = \frac{F_{x_c}}{\frac{1}{2}\rho_w S V_c^2}, \tag{4}$$

$$C_{y_c}\left(\chi_c\right) = \frac{F_{y_c}}{\frac{1}{2}\rho_w S V_c^2}, \tag{5}$$

$$C_{Mz_c}\left(\chi_c\right) = \frac{M_{z_c}}{\frac{1}{2}\rho_w S L_{PP} V_c^2}, \tag{6}$$

where ρ_w is the water density. For the moment M_{z_c}, also the length between perpendiculars L_{PP} is used to determine the non dimensional coefficients.

2.2. Proposed current model

The methods for the early-design stage are empirical, extremely simplified or assumed general while derived from a small set of specific vessels. With the scope of improving the current status of the early-design stage current loads evaluation, the present paper proposes to adopt higher fidelity methods to derive a surrogate model suitable for preliminary loads estimation. Viscous flow CFD calculations are an option for a more accurate prediction of current loads. The method is inappropriate for a direct application in the early design stage, even though the evaluation of current loads allows for the adoption of simplifications reducing the calculation time (e.g. neglecting Froude effects or unsteady phenomena). However, the execution of calculations on a validated set of calculation grids allows to obtain reliable data for the current on model-scale, with a fidelity level comparable to model tests. Since the computations are on model-scale, it is necessary to find a way to extrapolate the results on full-scale, which is of interest for station-keeping applications. As viscous phenomena mainly govern the current loads, it is possible to use a ship-model correlation line to scale the forces. Then, the resulting non-dimensional current coefficients for full-scale have the following expression:

$$C_{x_c}\left(\chi_c\right) = C_{F_f}\left(1 + k_x\left(\chi_c\right)\right) \tag{7}$$

$$C_{y_c}\left(\chi_c\right) = C_{F_f}\left(1 + k_y\left(\chi_c\right)\right) \tag{8}$$

$$C_{Mz_c}\left(\chi_c\right) = C_{F_f}\left(1 + k_{Mz}\left(\chi_c\right)\right) \tag{9}$$

where C_{F_f} is the full-scale friction line coefficient and the k values are determined according to the following relation:

$$k_i\left(\chi_c\right) = \frac{C_{i_{cm}}\left(\chi_c\right)}{C_{F_m}} - 1 \tag{10}$$

where C_{F_m} is the model-scale friction line coefficient and the $C_{i_{cm}}\left(\chi_c\right)$, with $i \in [x, y, Mz]$, are the model-scale current coefficients in the form of Eqs. (4) (5) and (6) predicted by means of CFD calculations. Therefore, the non-dimensional current coefficients in Eqs. (7), (8) and (9) represent a viscous resistance scaled to full-scale with a kind of *current form factor*.

By adopting this formulation, it is possible to derive a surrogate model for the $k_i\left(\chi_c\right)$ factors obtained by employing viscous flow CFD calculations and using, as an example, a friction line like the ITTC 57 ship model correlation. Such an approach implies the development of a database of CFD calculations performed on a set of hull forms covering a specific range of geometric parameters. Then the surrogate model for the $k_i\left(\chi_c\right)$ is a direct function of the geometric parameters of the source ships.

The following section describes the methodology and processes needed to develop such a surrogate model for current loads, using as a reference hull form a family of drill-ship.

3. Drill-ship database and design space

The starting point for developing the proposed current model is selecting the design space to cover, which means selecting reference hull forms and choosing the relevant geometrical parameters of interest with the respective ranges. To this end, firstly a selection of drill-ships main particulars has been extracted from the worldwide fleet. Secondly, analysing the available geometrical dimensions, the set of varying parameters has been selected together with the reference hull form for the CFD calculations. Hereafter, the specific stages of this process are described and discussed.

Table 1
Drill-ship main dimension database.

	L (m)	B (m)	T_d (m)	Δ (ton)	L/B (–)	B/T (–)	C_B (–)	$L/Vol^{1/3}$ (–)
1	238.0	42.0	11.9	104000	5.667	3.529	0.853	5.104
2	228.0	42.0	12.0	96273	5.429	3.500	0.817	5.016
3	228.0	42.0	12.0	96507	5.429	3.500	0.819	5.012
4	229.0	42.0	12.0	96000	5.452	3.500	0.811	5.043
5	229.0	42.0	12.0	96507	5.452	3.500	0.816	5.034
6	229.0	42.0	12.0	96000	5.452	3.500	0.811	5.043
7	230.0	38.0	11.0	78643	6.053	3.455	0.796	5.413
8	230.0	38.0	11.0	78463	6.053	3.455	0.796	5.417
9	230.0	38.0	11.0	77000	6.053	3.455	0.781	5.362
10	228.0	42.0	12.0	96000	5.429	3.500	0.815	5.021
11	230.0	36.0	11.0	70205	6.389	3.273	0.752	5.621
12	228.0	42.0	11.9	96000	5.429	3.529	0.822	5.021
13	218.0	42.0	12.2	90661	5.190	3.443	0.792	4.893
14	228.0	42.0	12.0	96000	5.429	3.500	0.815	5.021
15	228.0	42.0	12.2	90661	5.190	3.443	0.792	5.117
16	229.0	36.0	11.0	69900	6.361	3.273	0.752	5.605
17	228.0	42.0	12.0	97500	5.429	3.500	0.828	4.995
18	228.0	42.0	12.0	96142	5.429	3.500	0.816	5.018
19	238.0	42.0	12.0	103978	5.667	3.500	0.846	5.103
20	238.0	42.0	11.9	104184	5.667	3.529	0.854	5.100
21	228.0	42.0	11.9	87072	5.429	3.529	0.745	5.187
22	228.0	42.0	11.9	97978	5.429	3.529	0.839	4.987

3.1. Fleet database

There is a lack of availability of a reference database for drill-ship hulls in the open literature; therefore, it is necessary to refer to the data available on websites of shipping companies or shipyards, which usually report only general dimensions as the length L, the breadth B, the draught T and the displacement Δ. Such info is indicative, as, despite the breadth, it is not clear which specific L is reported (e.g. the length overall, the length between perpendiculars, etc...), which draught (e.g. design, operative, transfer, etc...) and if the displacement refers to the declared T. Hence, the available data are uncertain, but excluding unrealistic combinations of data, they are still a source for having a general overview of dimensions relevant to the early-stage design. Furthermore, the main dimensions allow for evaluating the principal non-dimensional quantities employed in ship design like L/B, B/T, C_B and $L/Vol^{1/3}$, with Vol the volume of the vessel. Here, the generic length L is interpreted as the length between perpendiculars, and the draught refers to the design draught T_d.

Analysing the actual fleet of drill-ships currently working worldwide, a set of about 40 vessels has been extracted for the study. However, due to the contracts between shipowners and yards, most of them are sister ships having the same general dimensions. Hence, eliminating the vessels with the same dimensional characteristics, a final number of 22 ships has been considered as the reference database. The available main geometrical characteristics of the drill-ships are listed in Table 1.

Fig. 2 shows an overview of the distributions of the main dimensional characteristics of the drill-ships database. The figure is composed of diagrams showing the pairwise distributions of L, B, T_d and Δ, together with their relative frequencies f in histogram form. From the diagram, it can be observed that most of the drill-ship population is distributed in a range of L between 225 and 230 metres, without a specific correlation with the other dimensions. Concerning breadth B, the large amount of the population has a value of 42 metres with a very small amount of outliers, all smaller than 42 metres. The design draught T_d is distributed around 12 metres with a smaller subpopulation of around 11 metres. Finally, the displacement is distributed with a peak of around 96 000 tons and has a uniform tail for smaller values. Also, in this case, no specific correlation is observed with other dimensional variables.

To have a broader overview of the database, it is worth considering also the non-dimensional variables. To this end, Fig. 3 shows the pairwise comparison of the non-dimensional geometric coefficients and the relative frequencies f in histogram form. The figure highlights only a strong correlation between L/B and $L/Vol^{1/3}$ due to the presence of L in both coefficients. However, looking more in detail at the database, the values of the non-dimensional coefficients are more evenly distributed across the design space interval.

Therefore, it is convenient to consider the non-dimensional coefficients as a starting point for developing the design space, giving a broader coverage of the database. Furthermore, it is necessary to define the interval of the parameters to cover the design space. For this purpose, two are the main issues to address:

- *Non-dimensional parameters selection*: from the database it is possible to determine the four non-dimensional coefficients reported in Table 1 and Fig. 3. However, the $L/Vol^{1/3}$ is linearly correlated with the L/B. Hence, for generating the design space it is better to consider only three parameters not showing evident correlations between each others, means taking into account L/B, B/T and C_B.
- *Block coefficient* C_B: from the drill-ship database some values for the C_B appear suspicious, as it is not reasonable to have a C_B lower than 0.8 for a drill-ship in operative conditions. Therefore, such ships should not be considered in the final selection of the design space boundaries.

Given the above, according to the shortened database, the following intervals have been chosen to perform the investigation:

$$5.00 \leq L/B \leq 6.80 \tag{11}$$

$$2.90 \leq B/T \leq 3.60 \tag{12}$$

$$0.83 \leq C_B \leq 0.90 \tag{13}$$

Based on these intervals, it is then necessary to properly define the parameter variations granting a suitable coverage of the selected design space.

3.2. Generation of the design space

The first step is to choose a suitable number of variations should be chosen along the design space limits to determine a systematic series of drill-ship hulls. To this end, proper methodologies have to be applied to select the sample ship parameters, remembering the application of a design surface methodology for the surrogate model development. Then, the Design of Experiments (DOE) allows for reducing the number of experiments that need to be executed, resulting in a lower effort

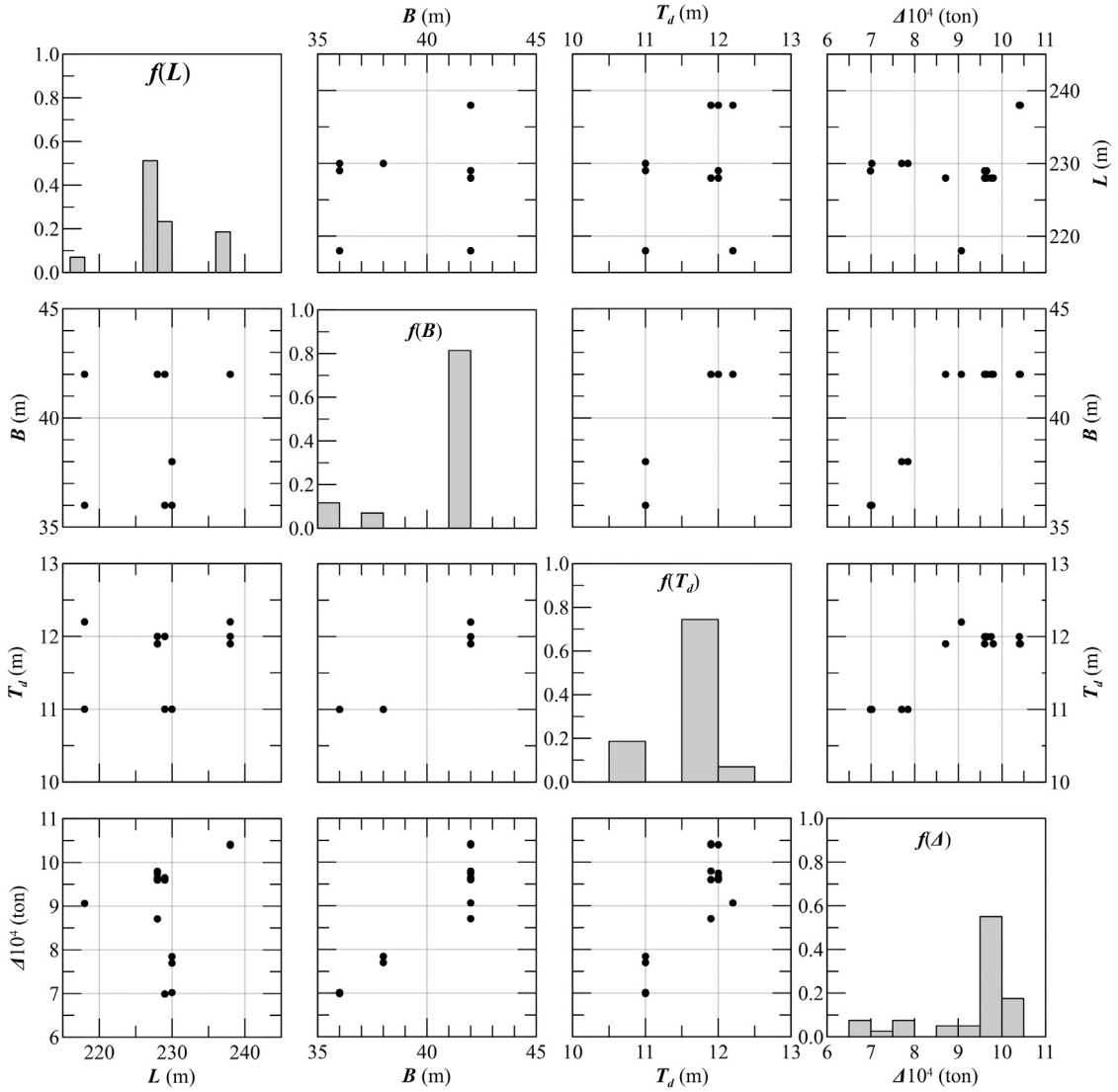

Fig. 2. Pairwise distributions and frequencies of dimensional characteristics for the drill-ship database.

for experimentation and calculation work (Chang, 2008). DOE is an aid to the response surface methodology and helps in quantifying the relationship between the controlled input parameters and the obtained surface response. The main process is as follows:

- Designing a series of experiments for adequate and reliable measurement of the analysed response.
- Developing a mathematical model of the response surface with the best fitting.
- Finding the optimal set of experimental parameters that produce the maximum or minimum value of a response.
- Representing the direct and interactive effects of process parameters through two or three dimensional plots.

Among the possible available choices for applying DOE techniques, the present study employs the Box-Behnken experimental design for finding the relationship between the hull parameters and the current forces. Box-Behnken design (Box and Behnken, 1960; Box et al., 1978) is a rotatable second-order design based on three-level incomplete factorial designs. The characteristic arrangement of the Box-Behnken design levels allows the number of design points to increase at the same rate as the number of polynomial coefficients. For three factors, as per the current study, the design can be constructed as three blocks of four experiments consisting of a full two-factor factorial design with the level of the third factor set to zero. In general, Box-Behnken is a spherical, revolving design. Viewed as a cube, it consists of a central point and the middle point of the edges. For the analysed problem, three variables are considered (L/B, B/T and C_B). Thus, 15 experiments are needed to cover the design space with a Box-Behnken model. Therefore, starting from the central point of the space corresponding to $L/B = 5.90$, $B/T = 3.25$ and $C_B = 0.865$, a set of 15 drill-ships has been generated employing an initial hull form provided by MARIN. The initial hull form (see Fig. 4 with reference to DRI_00) has a length of 220.0 metres, a breadth of 42.0 metres, a design draught of 13.0 metres and a displacement of 105 826 tonnes, leading to $L/B = 5.238$, $B/T = 3.231$ and $C_B = 0.878$.

Starting from the reference hull form, firstly, the hull DRI_15, representative of the centre of the design space, has been developed, scaling and adjusting the main dimensions and coefficients to meet the target values. All the other hull forms have been derived from DRI_15. The design space was chosen according to non-dimensional coefficient variations. However, to determine the calculation geometry, it is essential to define also the dimensional values of the reference hulls. For such a reason, it is mandatory to fix at least one of the dimensional values and change all the others according to the variations of the non-dimensional parameters. To this purpose, the value with less variability has been chosen as a fixed dimensional value, in this case, breadth B.

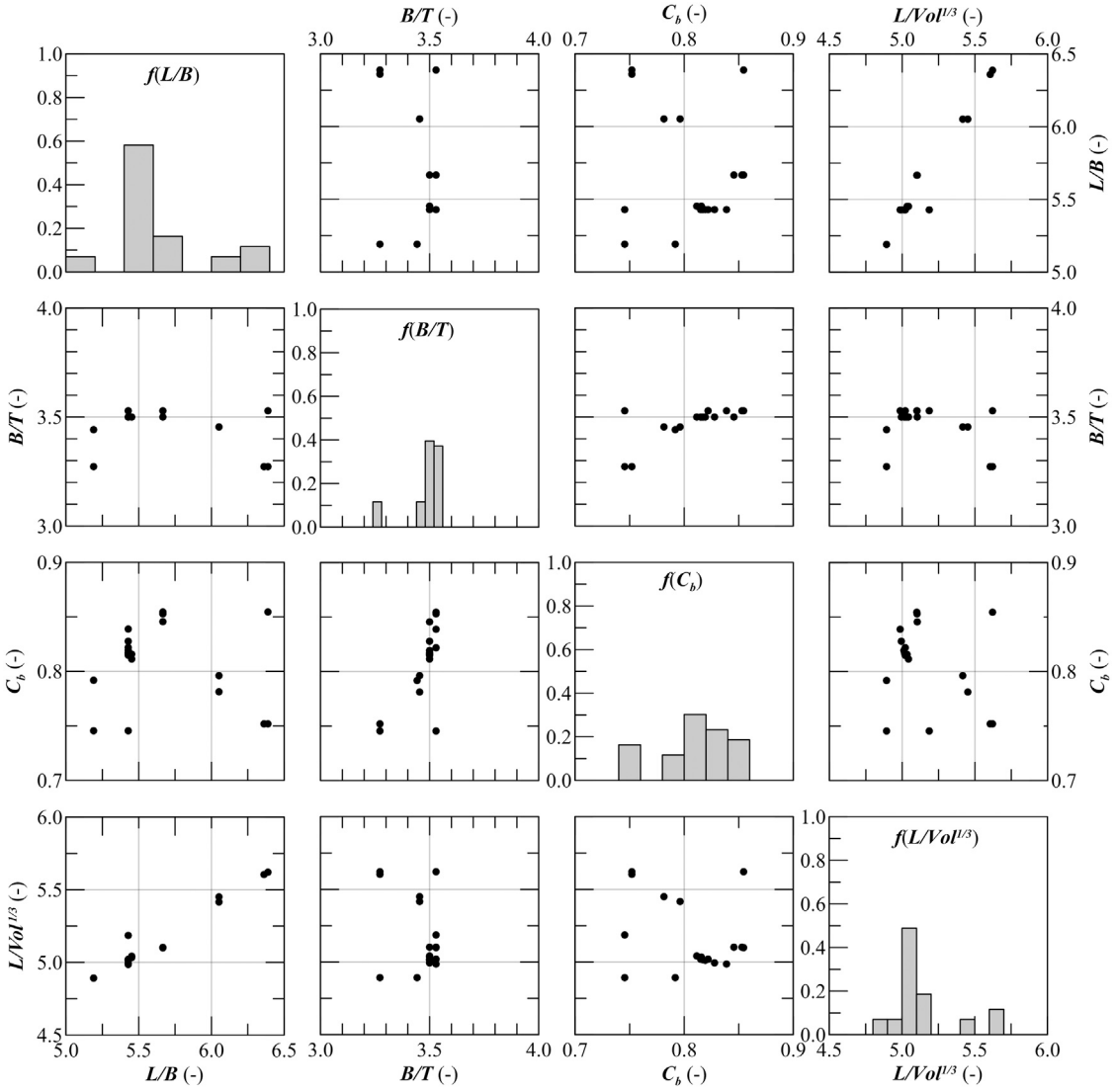

Fig. 3. Pairwise distributions and frequencies of non-dimensional characteristics for the drill-ship database.

Table 2
Drill-ship hull parameters according to Box-Behnken design.

	x_1 (–)	x_2 (–)	x_3 (–)	L/B (–)	B/T (–)	C_B (–)	L (m)	B (m)	T_d (m)
DRI_01	−1	−1	−1	5.00	2.90	0.830	210.0	42.0	14.483
DRI_02	−1	−1	1	5.00	2.90	0.900	210.0	42.0	14.483
DRI_03	−1	1	−1	5.00	3.60	0.830	210.0	42.0	11.667
DRI_04	−1	1	1	5.00	3.60	0.900	210.0	42.0	11.667
DRI_05	1	−1	−1	6.80	2.90	0.830	285.6	42.0	14.483
DRI_06	1	−1	1	6.80	2.90	0.900	285.6	42.0	14.483
DRI_07	1	1	−1	6.80	3.60	0.830	285.6	42.0	11.667
DRI_08	1	1	1	6.80	3.60	0.900	285.6	42.0	11.667
DRI_09	−1	0	0	5.00	3.25	0.865	210.0	42.0	12.923
DRI_10	1	0	0	6.80	3.25	0.865	285.6	42.0	12.923
DRI_11	0	−1	0	5.90	2.90	0.865	247.8	42.0	14.483
DRI_12	0	1	0	5.90	3.60	0.865	247.8	42.0	11.667
DRI_13	0	0	−1	5.90	3.25	0.830	247.8	42.0	12.923
DRI_14	0	0	1	5.90	3.25	0.900	247.8	42.0	12.923
DRI_15	0	0	0	5.90	3.25	0.865	247.8	42.0	12.923

As can be seen in Table 1, most of the vessels have a B of 42.0 metres. Then all the other main dimensions are varied accordingly. To properly define the final geometries, other parameters should be defined, such as, for example, the midship coefficient C_M and the position of the longitudinal centre of buoyancy LCB. Here it has been assumed to keep those two values constant in order to avoid effects of these two coefficients on the final forces. C_M has been selected equal to 0.98, and LCB has been set to −1.6% L_{PP}. Table 2 reports the resulting non-dimensional coefficients and the main dimensions for the 15 drill-ships composing the database. All the hulls have been generated starting

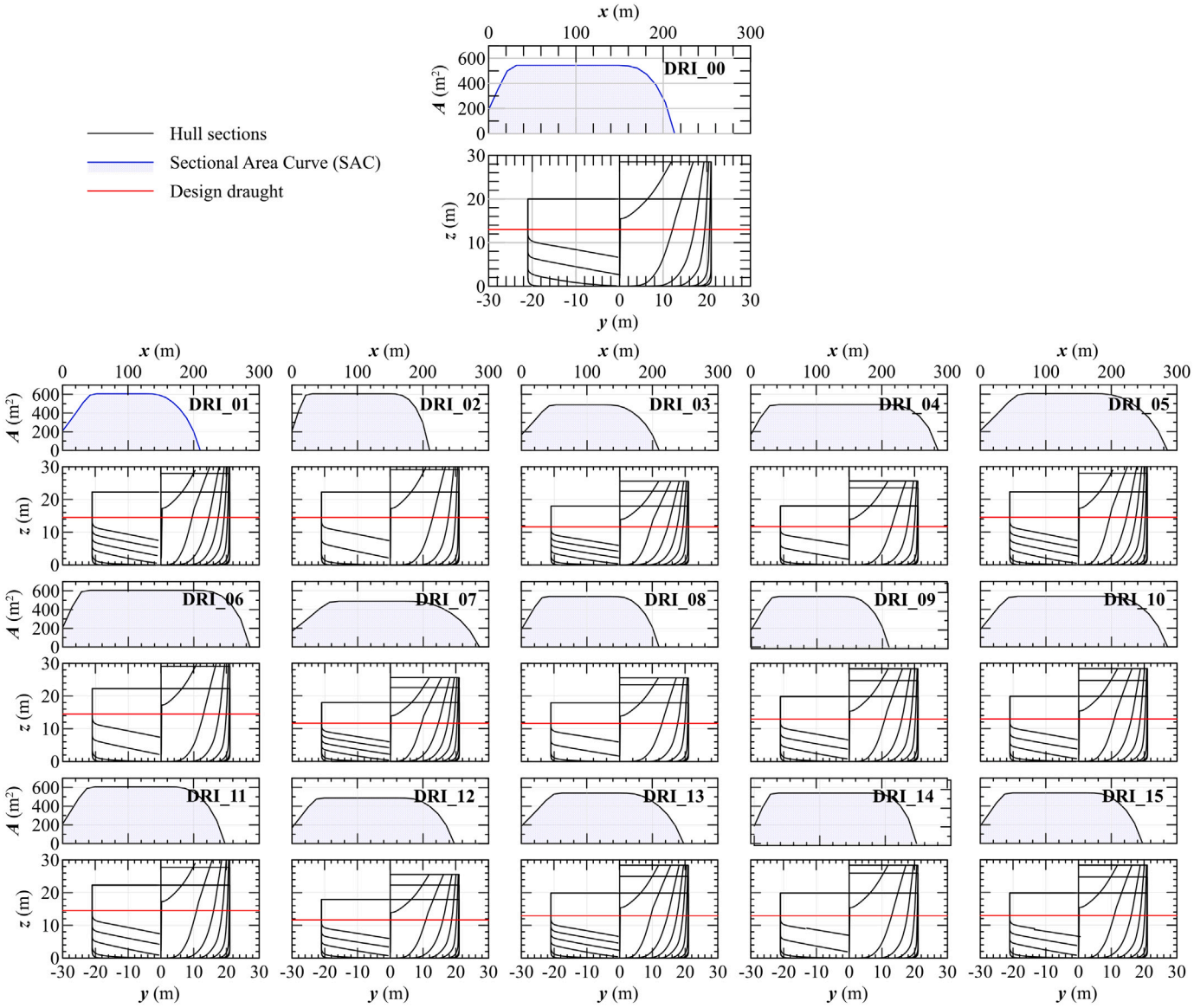

Fig. 4. Transversal sections and SAC of the reference hull form(DRI_00) and of the 15 hulls composing the database.

from the parent hull form. Fig. 4 shows the transversal sections and the Sectional Area Curve (SAC) of the 15 hulls. The family of drill-ships is likely a systematic series of hull forms (Todd, 1963; Roseman, 1987; Della Loggia and Doria, 1980; Swift et al., 1973; Bailey, 1976) composing the starting geometries for CFD computations and current model development.

4. Current model development

It is possible to implement the surrogate model for current loads based on numerical analyses, having defined the hull forms composing the drill-ships' design space. The upcoming sections describe the CFD calculations performed on the family of hulls. Afterwards, the multiple linear regression model is developed starting from the database of numerical results. Finally, the loads calculated with the obtained surrogate model are compared with standard current loads calculations on a reference drill-ship (DRI_00).

4.1. CFD calculations

CFD calculations allow for determining the forces along the hull, not only in a uniform flow oriented against the vessel in the heading direction but also for drift angle conditions. In such a case, the calculations evaluate the forces and moments generated on the hull by the current acting with a certain incidence angle and speed. Here, the calculations have been carried out at model-scale, simulating geometry models with a reference length of 8 metres on a calculation grid validated with model experiments on a high C_B hull form (Mauro, 2019). The following sections present the numerical models, the calculation domain and the obtained results for the current loads. The validation of the calculation domain and the numerical set-up are given in Appendix B, and refers to a Very Large Crude Carrier (VLCC) vessel where model test data are available in the literature for small heading angles. Appendix B includes also the mesh independence study at large heading angles performed with the same numerical set-up of the validation at small headings. Therefore, the calculation grid employed for the calculations on the drill ships is not directly validated but refers to a similar test case on a high C_B hull. Such an assumption is not influencing the reliability of the study at small heading angles, as the model-scale calculations refer to comparable Reynolds numbers. For large headings, no validation material is available. However, the mesh independence study ensure that the calculations are not affected by a relevant discretisation error for large headings, where flow separation occurs.

4.1.1. Numerical model

The modelling of the viscous flow around the hull has here been performed through Reynolds Averaged Navier–Stokes (RANS) equations. The resolution of the governing equations of continuity and momentum in viscous flow has been carried out employing STAR-CCM+ solver (STARCCM, 2022). In this case, the RANS equations have been solved with a segregated approach on algebraic multi-grids (Ferziger and Perić, 2002), with the Rhie-Chow interpolation scheme for pressure-velocity coupling (Rhie and Chow, 1983), while the control over the total solution is obtained applying the SIMPLE algorithm (Patankar, 1980). The reproductions of the turbulent fluctuations on the mean flow have been modelled using the approximation given by the realisable $k-\omega$ turbulence model (Wilcox, 1998) by adopting a two-layer formulation solving only a single equation for k in the near wall region and determining ω algebraically as a function of the wall distance.

Since the current speed is not so high to imply a Froude-dependent phenomenon, the double-body approximation has been employed, modelling only the immersed part of the hull shape. A second-order scheme has been considered for the fluid convection term and turbulence equation. In such a way, the numerical diffusion inside the calculation domain is reduced, leading to a more accurate estimation of the body forces. The implicit time step to adopt through the simulation, having selected a segregated approach, has been set according to specific indications given by the ITTC (ITTC, 2011). All the calculations have been carried out considering fresh water with density $\rho = 997.561$ kg/m^3 and dynamic viscosity $\mu = 8.887 \cdot 10^{-4}$ Pa s.

4.1.2. Calculation domain

The calculations have been executed on a 3-dimensional rectangular domain representing the so-called virtual towing tank. The calculation domain for standard resistance simulations assumes geometric symmetry on the vertical plane, which means that only half side of the vessel and tank are modelled. Once different inflow directions should be considered, this kind of simplification is no more valid, requiring the modelling of the whole ship and tank. A larger domain will increase the computational effort needed to perform the calculations since the total cell number is doubled compared to a standard resistance calculation.

A hexahedral non-structured grid has been adopted for all the simulations. Each hexahedron is generated by trimming the virtual towing tank, so the finite volume domain is generated by trimmed hexahedral cells. Near the vessel, a cylindrical overset region is created, having a diameter of $1.5L$ and centred in the vessel midship point O. This region is capable of rotating in such a way as to generate the initial domain for different χ_c angles. The overset region is not composed of a hexahedral grid but of a polyhedral one. This choice gives more flexibility while rotating the domain and could capture in a better way flow asymmetries. In the near-wall region, a prism layer mesh has been adopted to generate orthogonal prismatic cells in the boundary region close to the hull surface.

All the geometrical mesh generation parameters have been parametrised as a function of a reference length L, to make the domain discretisation easily scalable and usable for several geometries and speeds. Particular attention has been given to the prism layer thickness obtained from a geometrical progression of the first near-wall cell. The first-cell thickness has been determined in such a way as to have a target $y+$ value of around 55 through all the Reynolds numbers Re tested in this study.

In each case, a prism layer with a number of layers (Npl) equal to 8 and a stretching factor of 1.3 has been considered. Applying these settings, it is then possible to automatically build the mesh for every considered Re. Velocity inlet boundary conditions have been adopted for the domain sides, except for the symmetry plane (in this case, the Top boundary), where the symmetry condition is used, and the outlet boundary, where the pressure condition is considered. An overview of the calculation domain adopted through this study is presented in Fig. 5, highlighting the dimensions and the boundary conditions adopted. Besides, Fig. 6 shows the calculation grid near the ship, showing the transition between the rotating overset region and the fixed external virtual towing tank. It has to be noted that the reference system embedded in STAR-CCM+ (visible in Fig. 5) differs from the one adopted in the analyses (Fig. 1). Therefore, all the CFD results have been converted to the reference system employed for and current analyses. station-keeping

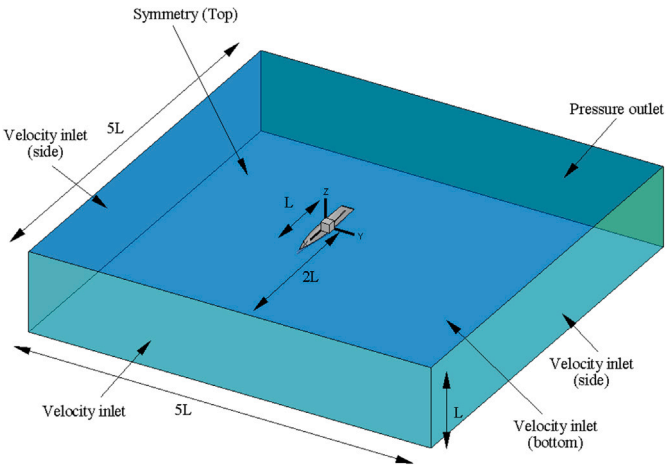

Fig. 5. Calculation domain dimensions and boundary conditions.

4.1.3. Results

Numerical simulations have been performed on the 15 drill-ships, employing the numerical set-up and the calculation grids described above and in Appendix B. The initial set of simulations for DRI_01 considers a higher number of encounter angles χ_c, simulating the following encounter conditions: 0.0, 5.0, 7.5, 15.0, 30.0, 45.0, 60.0, 75.0, 90.0, 105.0, 120.0, 135.0, 150.0, 165.0, 172.5 and 180.0 degrees. Such an initial test allows checking the encounter angle range to be refined for the calculations on the remaining hull forms, saving computational time. From the analysis, it has been decided to continue the study simulating the following 11 encounter angles: 0.0, 7.5, 15.0, 30.0, 60.0, 90.0, 120.0, 150.0, 172.5 and 180.0 degrees. Due to the differences between the STAR CCM+ solver and the adopted convention, the resulting angles in the two reference systems are opposite.

All the simulations have been initially performed until reaching a physical time of 20.0 s, with an implicit time step derived from the validation study (Appendix B), thus corresponding to 0.05 s following ITTC guidelines (ITTC, 2011). Every calculation requires about 6 h of computation on a laptop, employing 4 processes in parallel with a processor Intel Core i7-10750H CPU @ 2.60 GHz. All the computations reach a stationary value for the body forces at the end of the simulations.

As an example, Fig. 7 shows the time history of the forces on DRI_01 for a subset of encounter angles from 0.0 to 180.0 degrees in steps of 30.0 degrees. The forces F_x^* and F_y^* in the figure refer to a reference system fixed with the virtual towing tank; therefore, the body forces in the body fixed reference of Fig. 1 need the following rotation to be compliant with the reference system:

$$F_x = F_x^* \cos\chi_c - F_y^* \sin\chi_c \tag{14}$$

$$F_y = F_x^* \sin\chi_c + F_y^* \cos\chi_c \tag{15}$$

No action is needed for the moment M_z because the rotating domain is centred at the vessel midpoint, which is also the virtual towing tank reference system centre. Besides the forces, CFD simulations allow to visualise the pressure field along the hull, which is integrated along the body surface to find the final forces and moment acting on the hull.

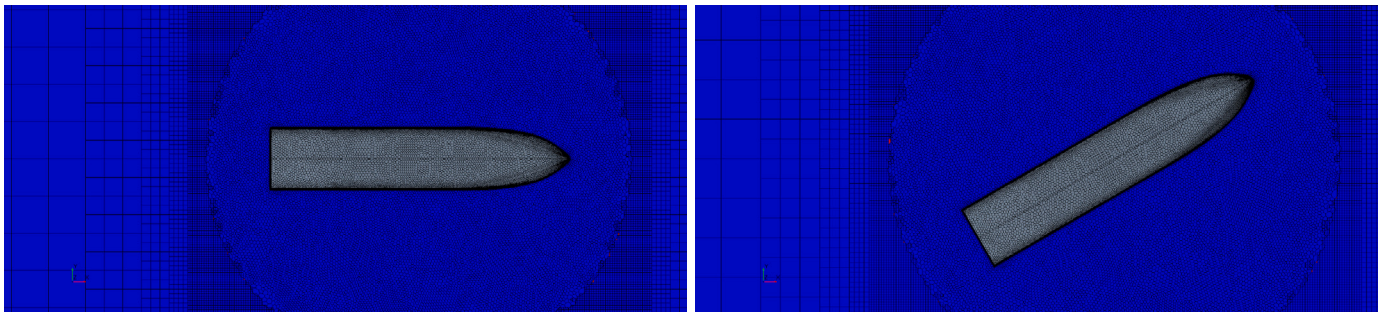

Fig. 6. Calculation grid for the angles χ_c=0 degrees (*left*) and χ_c=30 degrees (*right*) for DRI_01.

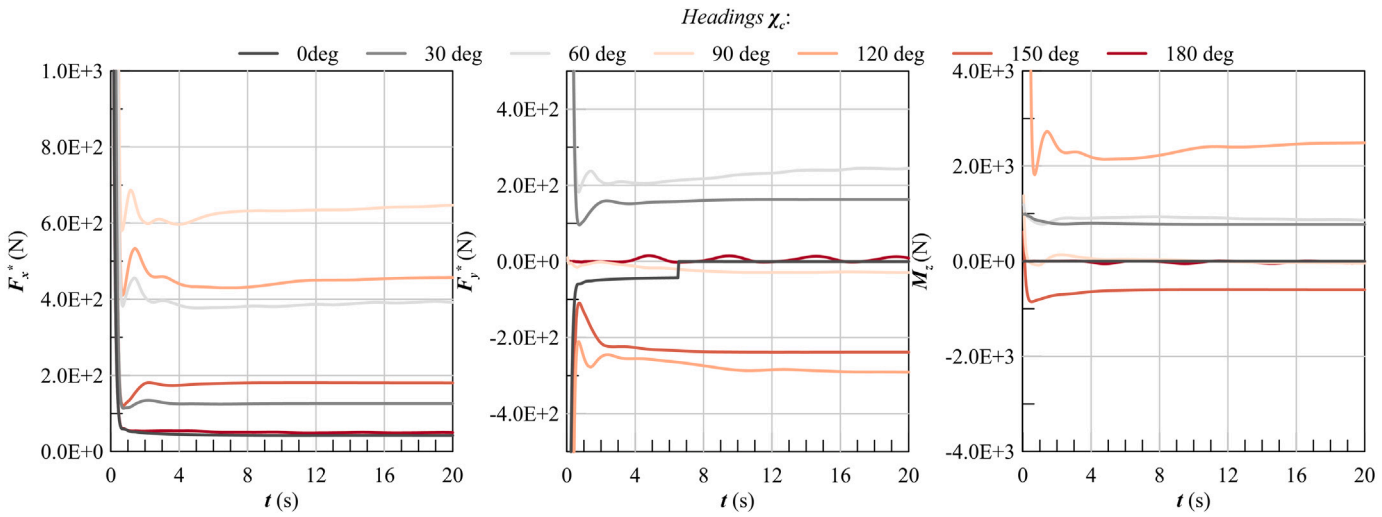

Fig. 7. Forces time history for DRI_01.

Fig. 8 shows an example on DRI_01, reporting the pressure field for the heading conditions from 30.0 to 180.0 degrees in steps of 30.0 degrees. It can be observed that the pressure field varies consistently with the encounter angle, highlighting asymmetries for headings far from the longitudinal direction and hemi-symmetries to 90.0 degrees. Such a behaviour of the pressure field influences the forces and moments acting on the hull, expecting a lateral force F_y as a function of the current direction symmetric to 90 degrees and a moment M_z hemi-symmetric to 90.0 degrees. The consideration on the longitudinal force F_x is different, as the totally different geometry between the bow and stern may lead to a non-smooth transition between 0.0 and 180.0 degrees. Fig. 9 shows the body forces and the moment for all 15 drill-ships in non-dimensional form. The figure confirms the trend supposed for the lateral force and the moment and allows to evaluate the behaviour of the longitudinal load, which has a double oscillation between 0.0 and 180.0 degrees; thus, a behaviour in line with the experimental curve presented by the OCIMF methodology reproduced in Fig. A.1. Besides the pure considerations on the coefficients curves shape, Fig. 9 allows for highlighting the differences between the different hulls. There are significant variations in the coefficients along the design space for both the forces and moment. To implement the model, it is, therefore, reasonable to search for a correlation between load coefficients and hull parameters through a regression analysis.

4.2. Regression model results

Applying the Box-Behnken methodology to design the experiments for the preliminary CFD simulation implies adopting a second-order model to develop the surrogate model for current loads. Furthermore, according to Eq. (1), the evaluation of the loads necessitates the knowledge of the ship's wetted surface S. Therefore, a second-order model for S is also needed. Appendix C reports the implementation of such models, keeping this section for the representation of the results only.

Table 3 reports the results of the regression analyses, providing the coefficients a_i, b_i and c_i. The Table also reports the goodness of the regressions using R^2 and R^2_{adj}, defined as:

$$R^2 = 1 - \frac{SSE}{SS_{tot}} \tag{16}$$

$$R^2_{adj} = 1 - (1 - R^2)\frac{n-1}{n-n_p-1} \tag{17}$$

with:

$$SSE = \sum_{i=1}^{n} \left(y_i - f_i\right)^2 \tag{18}$$

$$SS_{tot} = \sum_{i=1}^{n} \left(y_i - \bar{y}\right)^2 \tag{19}$$

$$\bar{y} = \frac{1}{n}\sum_{i=1}^{n} y_i \tag{20}$$

where n is the number of points to fit, y_i are the points to fit, f_i are the fitting values from the regression, and n_p is the number of coefficients in the regression. The use of R^2 as the sole indicator of the goodness of the fitted value is not suggested as, by increasing the number of regression parameters, the estimate can be not reliable. On the other hand, R^2_{adj} is an unbiased estimator of R^2 and is an adequate estimator for model fit, especially in the feature selection stage of multiple linear regression models. While performing the regression analyses, non-significant parameters have been discarded according to the associated variations on the R^2_{adj} while removing the variable from the regression model; more precisely, discarding terms with $\Delta R^2_{adj} \leq 0.001$. Table 3 also reports

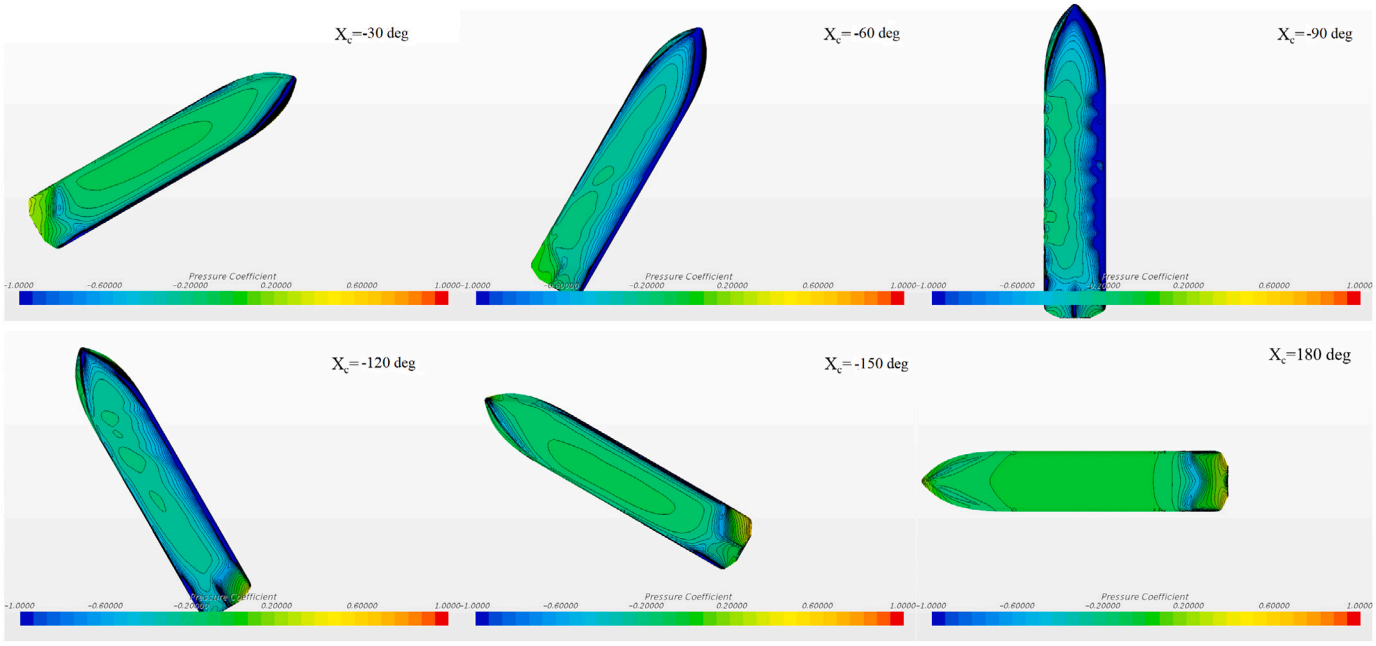

Fig. 8. Pressure coefficient at several heading angles for DRI_01.

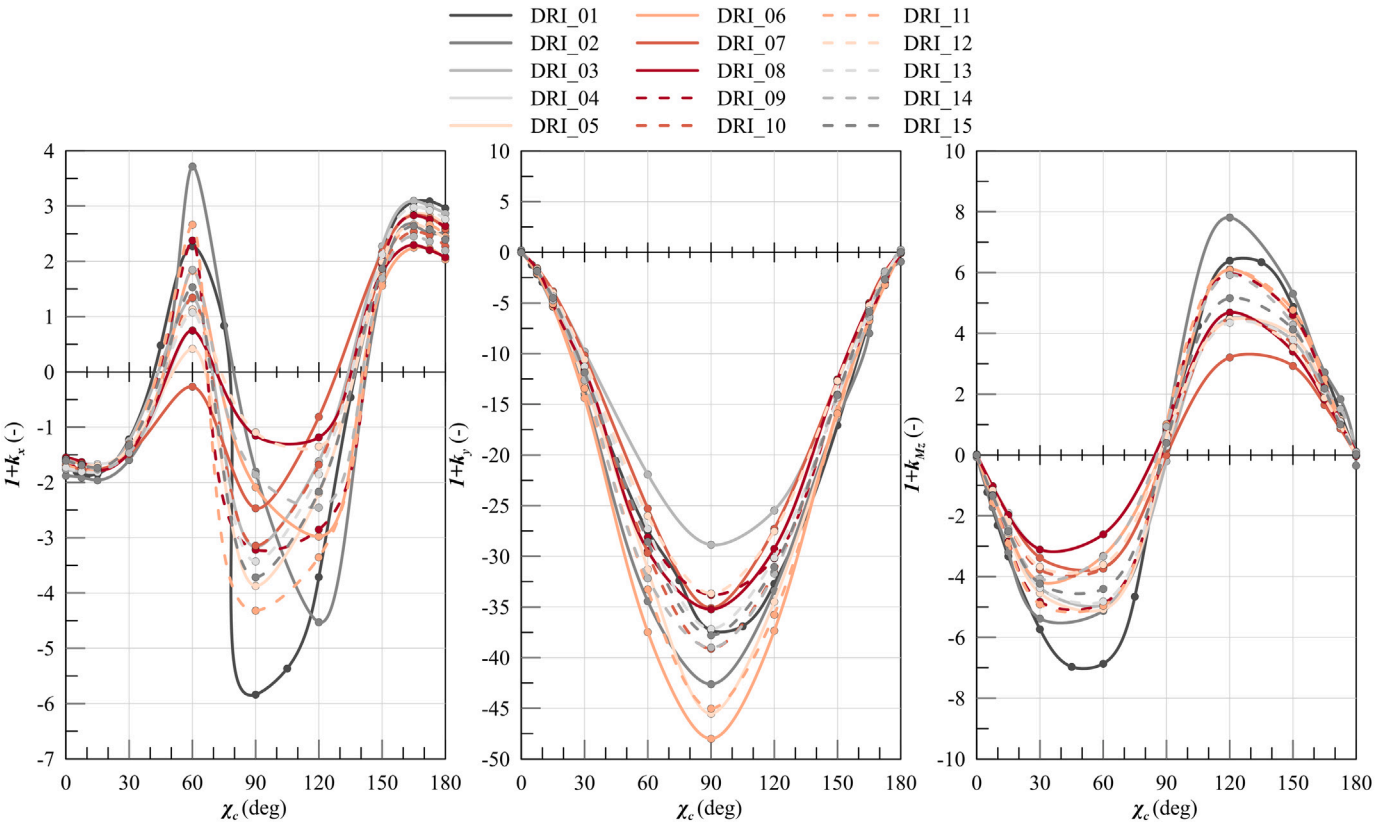

Fig. 9. Coefficients $1+k_x$, $1+k_y$ and $1+k_{Mz}$ for the drill-ship family according to CFD calculations.

the F statistics and the global p-value associated with the regression model, highlighting that all the regressions are significant to the initial data set.

It can be noted that, having selected a different regression per each angle, the obtained statistical values are quite high, always above 0.8 for R^2 and above 0.7 for R^2_{adj} for the k_x. Such a consideration is also valid for k_y and k_{Mz}, except for angles close to 0.0 and 180.0 degrees, where R^2 values are below 0.7. Figs. 10–12 show the results of the proposed regression model with the CFD calculations for all 15 drill-ships of the design space. From the figures, it is evident that the regressions capture the trend of the CFD-derived coefficients through the whole set of headings. For the k_x, differences between CFD and regression curve are more evident for headings around 90.0 degrees for DRI_01, DRI_04, DRI_11, DRI_13 and DRI_14. This happens because the

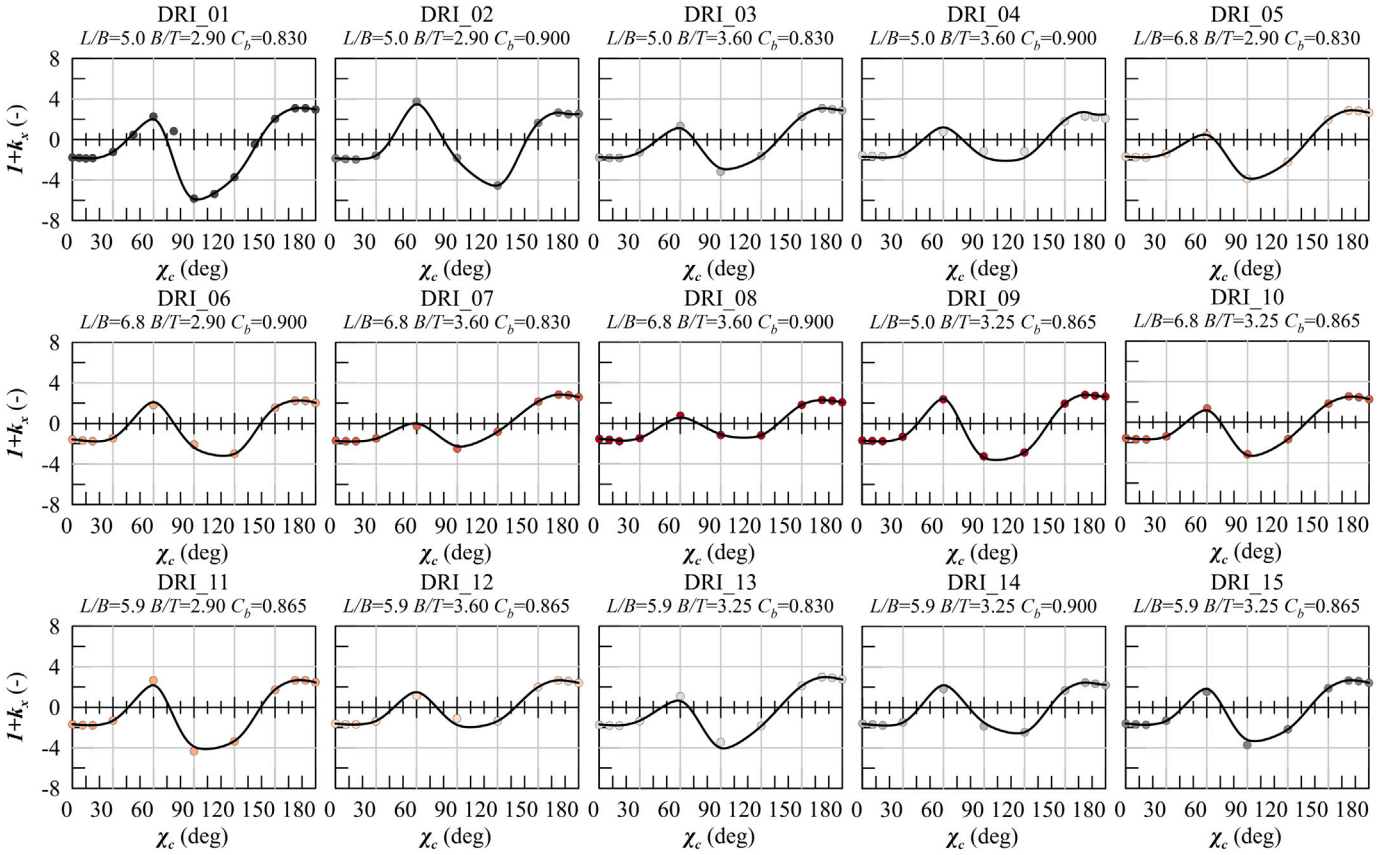

Fig. 10. Coefficient $1 + k_x$ for the drill ship family according to calculations (*dots*) and to proposed regression model (*continuous*).

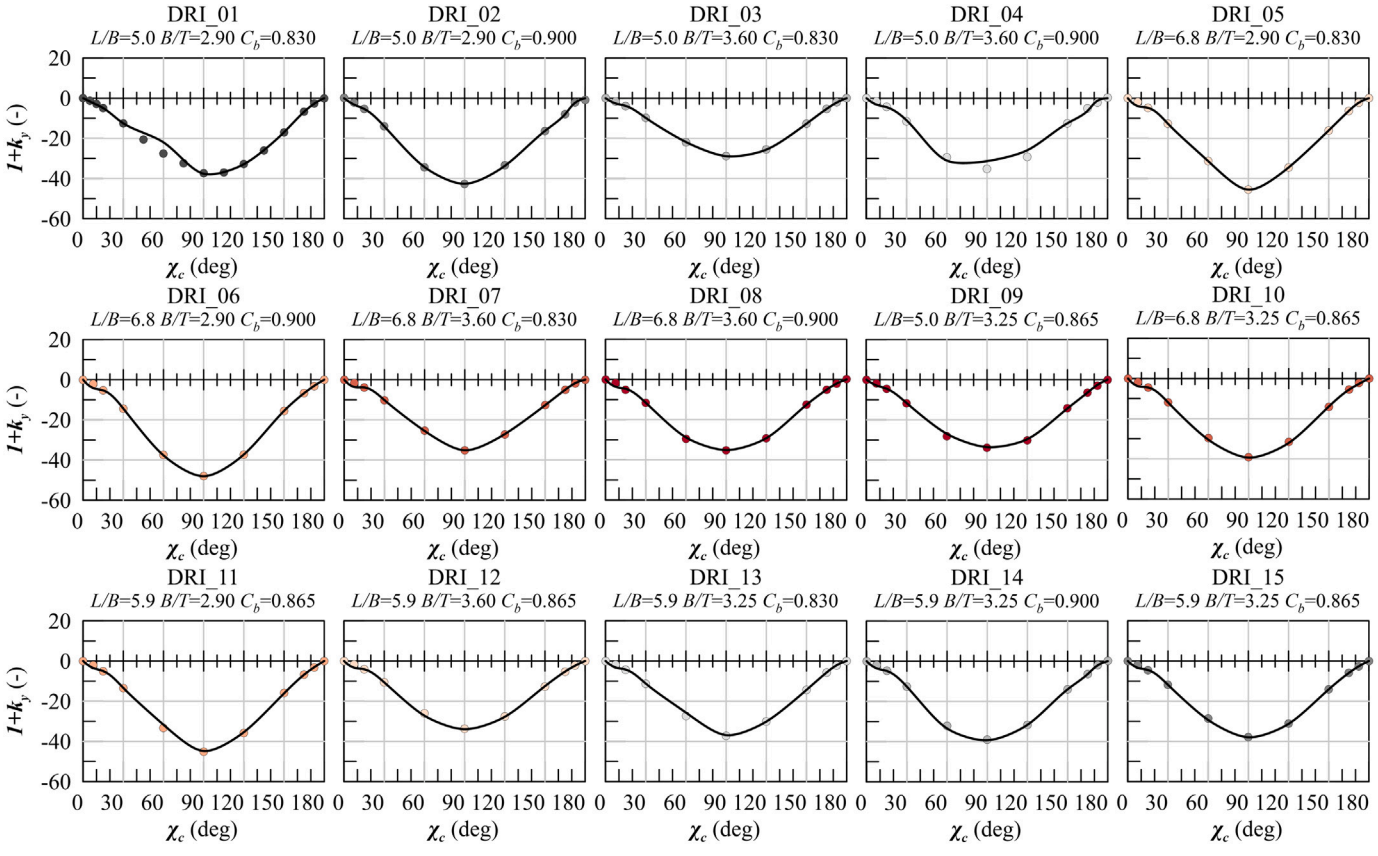

Fig. 11. Coefficient $1 + k_y$ for the drill ship family according to calculations (*dots*) and to proposed regression model (*continuous*).

Table 3
Regressions coefficients and goodness of fit for k_x, k_y and k_{Mz}.

	χ_c(deg)										
	0.0	7.5	15.0	30.0	60.0	90.0	120.0	150.0	165.0	172.5	180.0
a_0	19.1257	17.0836	33.6589	20.7580	502.6692	−85.5921	−41.7396	−27.7743	−4.9685	−12.4991	−32.7693
a_1	0.0269	0.1258	−0.4661	1.5525	0.5089	−10.4121	−6.1345	0.6715	0.6167	1.1852	0.8440
a_2	2.3027	2.1981	1.2096	1.7329	−35.6461	−24.2347	−0.1425	−1.0639	−1.7416	−0.7600	−0.8712
a_3	−47.0108	−42.6690	−74.3122	−64.5073	−1.0285e3	403.2347	153.1344	54.3124	−1.9143	7.3382	57.5958
a_4	0.1286	0.0992	0.1341	0.0999	–	–	0.8982	–	−0.1492	−0.2335	−0.2095
a_5	−0.5873	−0.5714	–	−2.1307	–	11.7220	3.0686	−0.4889	–	−0.7749	–
a_6	−3.6735	−3.3469	−2.4490	−2.6470	42.9976	25.3908	−16.9647	–	3.1408	1.8989	2.6389
a_7	–	–	–	–	–	–	–	−0.0175	–	–	–
a_8	–	–	–	–	–	–	0.9977	0.1143	–	–	–
a_9	35.2653	32.2449	47.4286	50.7800	504.1007	−338.4658	−63.5680	−26.3115	–	–	−33.4554
F	7.9841	8.2643	7.7558	30.4866	10.7656	10.5622	82.9452	165.4151	48.0253	89.3391	38.3470
p-val	0.0068	0.0062	0.0054	9.9895e−5	0.0014	0.0018	1.4104e−5	3.0964e−7	3.2026e−6	6.8497e−7	1.8109e−5
R^2	0.8887	0.8921	0.8533	0.9682	0.8568	0.8907	0.9910	0.9940	0.9639	0.9853	0.9664
R^2_{adj}	0.7774	0.7841	0.7433	0.9365	0.7772	0.8087	0.9791	0.9880	0.9438	0.9743	0.9412
b_0	–	−51.4523	115.7433	74.5229	−590.4896	−110.5882	64.6027	158.1107	−28.5981	−203.6984	–
b_1	–	4.9007	−4.2514	1.2665	53.1941	60.0397	6.0102	−2.4902	−2.1344	−5.7252	–
b_2	–	9.0851	−14.7326	−11.8586	90.4234	−89.2599	−20.3454	−29.4760	9.6351	−0.9192	–
b_3	–	52.6873	−177.5060	−117.6775	637.7501	257.9824	−42.2293	−179.4784	64.0150	521.9401	–
b_4	–	−0.2560	0.3738	−0.1094	−4.1066	−2.9196	−1.5449	0.6975	0.5546	–	–
b_5	–	−3.1944	3.5952	−0.8966	−43.6733	−35.9117	–	–	–	6.5815	–
b_6	–	−9.1939	6.3673	–	−84.7521	–	22.5350	9.5848	−17.8265	–	–
b_7	–	−0.1053	–	–	–	−1.4147	–	–	–	–	–
b_8	–	–	0.8875	1.3397	–	14.1667	–	1.8433	–	–	–
b_9	–	–	83.4402	83.7693	–	–	–	82.7688	–	−323.3962	–
F	–	4.5593	13.7995	296.4824	24.0222	85.6513	63.7206	162.8032	47.2317	3.5315	–
p-val	–	0.0316	0.0024	4.0753e−8	1.0526e−4	3.0069e−6	9.4419e−7	3.2720e−7	3.4400e−6	0.0482	–
R^2	–	0.8201	0.9485	0.9966	0.9474	0.9885	0.9725	0.9939	0.9633	0.6624	–
R^2_{adj}	–	0.6402	0.8789	0.9933	0.9080	0.9769	0.9573	0.9878	0.9429	0.4748	–
c_0	–	−64.6197	20.8049	27.4603	14.4108	−41.5657	−10.8900	61.2539	1.7871	−85.1080	–
c_1	–	−0.0923	−3.7269	−5.6273	−10.1035	−2.1688	9.0724	5.0503	2.5305	−0.4180	–
c_2	–	6.5229	−0.3240	1.6986	−8.0568	21.3136	−4.3397	−4.6070	0.3871	2.5438	–
c_3	–	130.8021	−6.7438	−3.3814	113.2479	36.7484	−29.2297	−173.0483	−32.0710	187.0608	–
c_4	–	–	0.3702	0.5623	0.9788	−0.3271	−0.9451	−0.3425	−0.1975	−0.3523	–
c_5	–	–	2.5992	3.8238	5.1962	–	−6.1104	−4.1051	−1.9801	1.9797	–
c_6	–	−8.0981	−3.4796	−8.1493	–	−14.1338	14.5269	9.7855	1.9857	–	
c_7	–	–	–	–	0.1485	0.2825	–	–	–	–	
c_8	–	–	–	–	–	−1.0533	–	–	–	–	
c_9	–	−60.2449	–	–	−97.2406	–	–	92.8578	21.2404	−116.1291	–
F	–	6.3214	48.5822	52.6634	63.4103	9.3137	86.9986	53.4764	141.7022	4.3750	–
p-val	–	0.0087	7.3139e−6	5.3586e−6	8.4253e−6	0.0043	7.6002e−7	1.5058e−5	5.2926e−7	0.0296	–
R^2	–	0.7784	0.9733	0.9753	0.9845	0.9030	0.9849	0.9816	0.9930	0.7664	–
R^2_{adj}	–	0.6552	0.9533	0.9568	0.9689	0.8061	0.9736	0.9633	0.9860	0.5912	–

coefficient changes the sign in correspondence with that angle range, and such a phenomenon is difficult to be captured by the proposed regression model. For k_y, the regression quality is higher than k_x, and differences with CFD computations are evident only for DRI_01 around 70.0 degrees and DRI_04 around 90 degrees. For k_{Mz}, only DRI_04 presents some in-congruence with CFD data around 30 degrees. Further improvement could be probably reached by increasing the regression, considering dependencies higher than the second-order; however, that means an increase in the initial vessel population. In fact, the Box-Behnken methodology for the DOE is a limitation of the regression order. However, an additional option could be changing the regression type by employing auxiliary functions to approximate the coefficients, providing a regression for the function coefficients. However, such an option needs dedicated studies.

4.3. Comparison with conventional methods

The present method is derived from high-fidelity CFD computation on the set of drill-ships, which means it can capture the peculiarities of the coefficient curves across the whole range of headings. It is then of high interest to compare the loads derived from the proposed method with the conventional approaches presented in Appendix A, particularly with API and DNV methods.

Here, the original drill-ship DRI_00, which is not part of the 15 drill-ships composing the database, is used as a reference for the loads' calculation with the three different methods, together with the results of CFD calculation extrapolated to full-scale using Eqs. (7), (8) and (9). The main dimensions of DRI_00 are reported in Section 3.2, together with the non-dimensional coefficients. Even though the vessel is not part of the database, the non-dimensional coefficients are within the investigated design space; thus, the hull is suitable for being assessed with the regression model. Fig. 13 shows the results obtained by applying API, DNV, CFD calculations and the proposed regression model. Calculations have been performed imposing a current speed $V_c = 2.0$ m/s. The results highlight the good agreement between the CFD computations and the regression model. Differences within 5% can be observed for the longitudinal force only around headings close to 180.0 degrees, for the lateral force around 60 degrees and around 20–70 degrees for the moment.

On the other hand, the differences with the conventional load estimation processes are remarkably consistent. The API methodology always overestimates the forces (no model describes the moment), while the DNV method underestimates the loads. Therefore, the proposed regression model is a notable enhancement for the initial prediction of current loads on drill-ships.

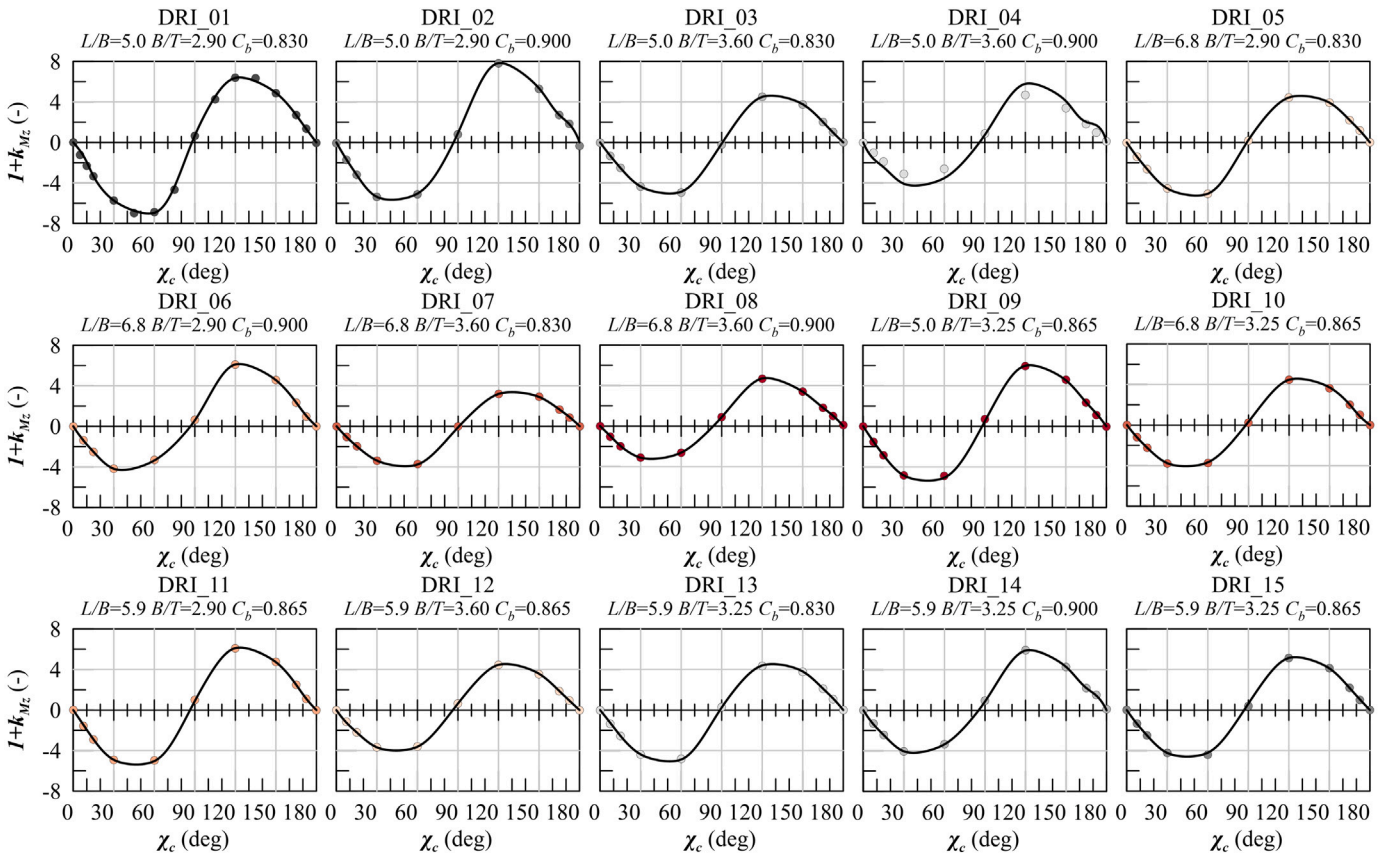

Fig. 12. Coefficient $1 + k_{Mz}$ for the drill ship family according to calculations (*dots*) and to proposed regression model (*continuous*).

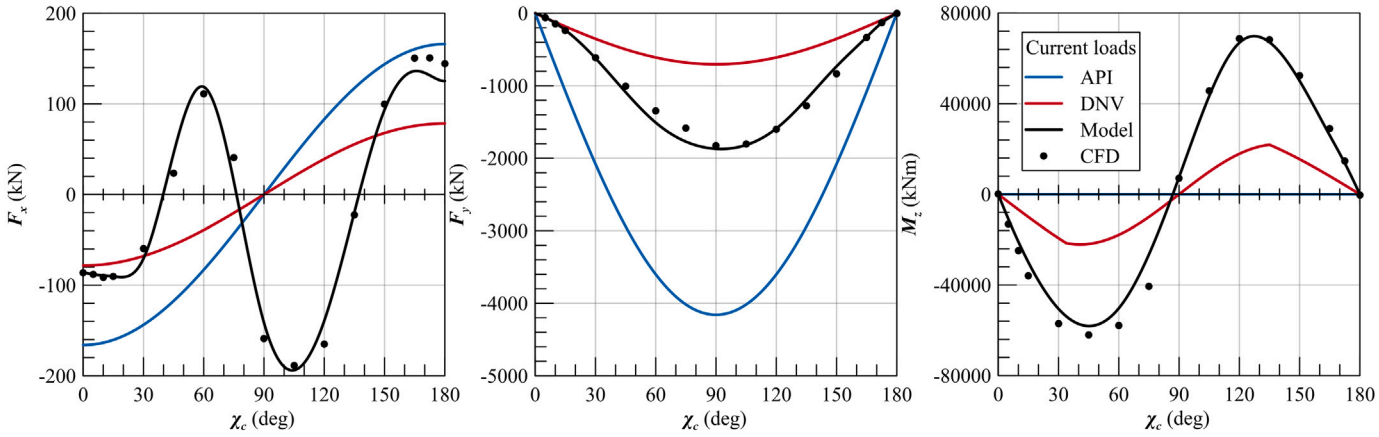

Fig. 13. Environmental loads for DRI_00 according to API, DNV and the proposed model.

5. Effect on polar plots

The comparison with traditional methods for current load estimation highlighted the improvement of the proposed surrogate model in capturing the behaviour of the loads with the encounter angle χ_c. As such, it is expectable that also the station-keeping prediction may be affected by the different environmental modelling. For this purpose, DP calculations have been carried out on DRI_00 to obtain the capability plot showing the maximum current speed the system can handle at different encounter angles in a given sea state by employing the analysed current models. Such a capability plot differs from the standard capability plots (IMCA, 2000), where the current is kept constant, and wind and waves vary according to a given correlation. Here, constant wind and wave are assumed, varying the current speed and considering all the loads concurrent with χ_c.

As a first step, a thruster layout, based on the almost standard configurations employed onboard these kinds of units, has been selected for the reference drill-ship. Table 4 reports the positions and sizes of the azimuth thruster units. The configuration is symmetric to the vessel's longitudinal plane, with all the thrusters capable of delivering the same maximum thrust. Therefore, the resulting capability plot will be symmetric between the headings χ_c of 0–180 and 180–360 degrees.

Recalling the description of the quasi-static DP problem in Section 2, a self-developed tool (Mauro and Nabergoj, 2015, 2016; Mauro and Prpić-Oršić, 2020) has been employed to solve the equilibrium system of Eq. (1) using a non-linear optimisation algorithm based on recursive quadratic programming (Arditti et al., 2015, 2019; Mauro and

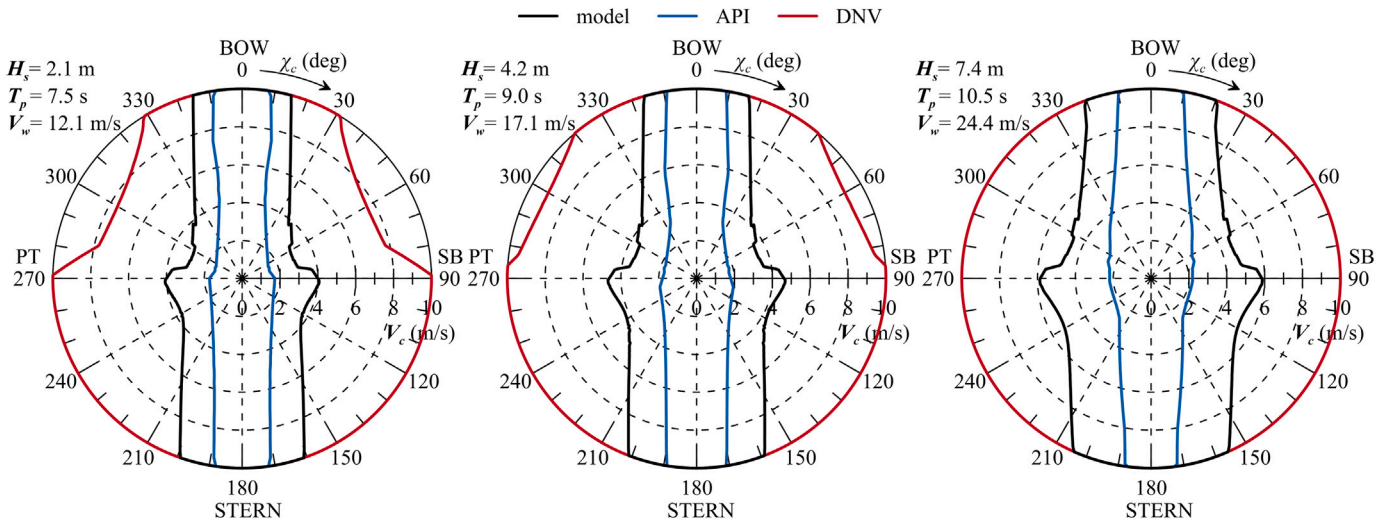

Fig. 14. Current capability plots according to API, DNV and regression model loads.

Table 4
Thrusters position and size for drill-ship DRI_00.

ID	x_a (m)	y_a (m)	D (m)	$f_{a_{max}}$ (kN)
THR_1	90.0	0.0	3.9	902.2
THR_2	75.0	−16.0	3.9	902.2
THR_3	75.0	16.0	3.9	902.2
THR_4	−92.5	−16.0	3.9	902.2
THR_5	−92.5	16.0	3.9	902.2
THR_6	−105.0	0.0	3.9	902.2

Duranti, 2018). The solver handles multiple sources of environmental loads (Mauro and Nabergoj, 2022), thus, evaluates the DP capability according to the current loads f_c provided by API, DNV and novel regression procedure. Calculations have been performed employing the DNV methodology for early design (DNV-GL, 2018) for the estimation of wind f_W and wave f_w loads. Three fixed combinations of wind and waves have been selected from the wind-wave correlation proposed by DNV (DNV-GL, 2018), corresponding to $H_s = [2.1, 4.2, 7.4]^T$ metres, $T_p = [7.5, 9.0, 10.5]^T$ seconds and $V_W = [12.1, 17.1, 24.4]^T$ m/s, respectively.

Fig. 14 shows the capability results according to the mentioned methodologies for the current loads and environmental conditions. It can be observed that the differences highlighted by the current loads in Fig. 13 reflect the capability plots. Employing the DNV method reflects in the higher capability for all three tested environmental conditions. On the other hand, the API methodology estimates the lower capability, showing the lower sustainable current speed for all the tested sea states and headings. The proposed methodology based on regressions estimates a maximum sustainable current speed between the two conventional methods, showing a different behaviour along the headings compared to the other predictions performed with Class rules. Such a result is mainly due to the shape of the environmental coefficients across the headings, especially concerning the longitudinal force F_{X_c} and yawing moment M_{Z_c} modelling.

For such reasons, the current load modelling with the proposed regression-based method based on model-scale CFD computation scaled according to a current form factor is representative of a significant enhancement to the early design procedures available in the literature. Furthermore, the calculation time necessary for the current load estimation during DP capability analysis is the same for all the presented methods, thus, the methodology complies with the designers' fast calculation time necessities.

6. Conclusions

The present work reports a model for the fast and reliable prediction, in the early design stages, of current loads acting on a drill ship during station-keeping operations. The model employs a surrogate model, built with Multiple Linear Regressions based on a database of CFD calculations instead of using empirical assumptions or extremely simplified formulations. The model considers the current coefficient as a form factor, derived by CFD computations, times a friction coefficient, evaluated with ITTC-57 friction line. The scale effect is included in the frictional component of the forces, as confirmed by several numerical studies on resistance and current loads. Therefore, CFD computation have been performed on model-scale using calculation grids and numerical setups validated on comparable geometries. The calculations reported in the present study refer to calculation grids validated for small heading angles. This is a limitation for the reliability of the final results but having ensured the independence of the grid for large headings decreases the final uncertainties of the method, which for sure needs further validation at large heading angles. However, even considering only the mesh independence for large headings, such a strategy increases the reliability and fidelity of the method compared to the standard evaluation methods available in the literature.

By comparing the results on reference drill-ships, it is evident that the developed method can capture the behaviour and magnitude of the current loads acting on the vessel. Furthermore, the adoption of the enhanced current loads influences the station-keeping capability of the vessel, as highlighted by the capability plots presented in this study. Thus, the higher fidelity model developed affects the initial DP predictions and, consequently, the design of the whole vessel. That means the developed model is an enhancement for the early design stage of drill-ships.

The method uses some simplifications. The method considers drill-ships with a bare-hull condition, thus, neglecting appendages. Drill-ships may have negative appendages: the moon-pools. Even though the effect of the moon-pool is more significant for the transit case, the impact on the current loads should be checked in any case. Furthermore, aiming at developing the method for other hull forms, the consideration of appendages is extremely important for other offshore vessels (e.g. stingers for pipe lay vessels) and passenger vessels or pleasure crafts. Then, the presence of rudders, struts, and bow/stern tunnels may influence the final forces. In case appendages should be relevant, the numerical assumptions may be too simplified and unsteady flow simulations could be necessary for developing a CFD database. Such a matter requires the execution of a dedicated validation

study on a different calculation grid than the one presented in this study. Furthermore, the Box-Behnken methodology for DOE implies adopting a second-order model for the regressions, being a limitation to the accuracy of the model. Increasing the number of samples may allow for a higher-order regression mode or approximating functions for headings can be used instead of single regressions for each angle.

In conclusion, the present study proposes a methodology that is independent from the source and reliability of the CFD calculations. This, in turn, is a good starting point for a process that can be applied to different families of vessels and different vessel types, improving the reliability of current prediction in the early design stage, thus helping designers in having a better understanding of the station-keeping ability of a new design.

CRediT authorship contribution statement

Francesco Mauro: Conceptualization, Methodology, Software, Investigation, Formal analysis, Writing – original draft, Writing – review & editing. **Enrico Della Valentina:** Writing – review & editing. **Victor Ferrari:** Writing – review & editing. **Ermina Begovic:** Writing – review & editing.

Declaration of competing interest

The authors declare that they have no known competing financial interests or personal relationships that could have appeared to influence the work reported in this paper.

Data availability

Data will be made available on request.

Appendix A. Conventional methods for current loads estimation

A.1. API method

The method proposed by API (API, 1984) is a simple approximation. The document itself states that once more reliable data are present, those should be used for current force determination. In the absence of reliable data, the following formulations describe the maximum longitudinal and transversal loads:

$$F_{x_{cMAX}} = C_{cx} S V_c^2, \tag{A.1}$$

$$F_{y_{cMAX}} = C_{cy} S V_c^2, \tag{A.2}$$

where the dimensional coefficients C_{cx} and C_{cy} are 2.89 and 72.37 Ns^2/m^4, respectively. Afterwards, the forces can be distributed across the headings through simple sinusoidal rules. No specific indication is given for the determination of the yawing moment.

A.2. DNV method

The DNV guidelines for DP predictions (DNV-GL, 2018) present a simplified general method for current load estimation. The approach is not oriented to the determination of non-dimensional coefficients but estimates the forces as a function of the vessel's main particulars, usually available during the early stage of design.

The forces are given in the following form:

$$F_{x_c} = \frac{1}{2}\rho_w V_c^2 B T \left(-0.07 \cos \chi_c\right), \tag{A.3}$$

$$F_{y_c} = \frac{1}{2}\rho_w V_c^2 A_{L_c} \left(0.60 \sin \chi_c\right), \tag{A.4}$$

$$M_{z_c} = F_{y_c} \left[s_{L_c} + \max\left(c_c, -0.2\right) L_{PP}\right], \tag{A.5}$$

$$c_c = \min\left[0.4\left(1 - 2\frac{\chi_c^*}{\pi}\right), 0.25\right], \tag{A.6}$$

where the water density ρ_w should be 1026 kg/m^3, and s_{L_c} is the centre of the submerged lateral area with respect to the origin O. The parameter c_c is a function of an auxiliary heading angle χ^* expressed as:

$$\chi_c^* = \begin{cases} \chi_c & \text{if } 0 < \chi_c < \pi \\ 2\pi - \chi_c & \text{if } \pi \le \chi_c \le 2\pi \end{cases}, \tag{A.7}$$

It is also specified that the current method is suitable to determine loads once the current speed is low enough to maintain the Froude number evaluated on vessel breadth B under the value of 0.1.

A.3. OCIMF method

The guidelines provided by OCIMF (OCIMF, 1994, 2010) consist of adopting a fixed set of coefficients determined on VLCCs (Very Large Crude Carrier) with a displacement between 140,000 and 400,000 tons for full and ballast draughts. Those coefficients are considered suitable also for smaller units with displacement above 16,000 tons. The coefficients have been determined on model-scale distinguishing two different bow forms: conventional and cylindrical. Furthermore, data have been collected for different water depths d, providing reference curves for d/T ratios ranging between 1.1 and 4.0. Fig. A.1 shows the longitudinal force coefficient C_{xc}, the lateral force C_{yc} and moment C_{xyc} coefficients for infinite depth reported in OCIMF (1994), according to OCIMF nomenclature and reference system. From the figure, it can be noticed that the behaviour of coefficient C_{xc} presents more than one oscillation between negative and positive values, something not possible to capture with the above-described standard methods but achievable by employing CFD computations (Vroegrijk, 2017; Koop, 2015).

Appendix B. Verification and validation of CFD calculations on a standard geometry

Before executing the calculation on the drill-ship geometries, a validation study has been carried out to study mesh independence and the total uncertainty of the forces evaluation procedure. Aiming to ensure that the simulations have a satisfactory grade of accuracy, it is essential to perform this kind of study to establish the reliability of the adopted code and settings on similar geometries. Such a process is possible for conditions where experimental data are available but can be useful also to ensure mesh independence for cases where validation material is not available.

The determination of errors and uncertainties in the total process is of primary importance in determining the reliability of the obtained results. Error is intended as the difference between the obtained result of the computation and the one coming from experiments. On the other hand, uncertainty defines an interval containing the true value within a certain degree of confidence.

The numerical error δ_{SN} is the first focus of a validation study; this one can be divided into three different categories (Roache, 1998): the round-off error, the iterative error δ_I and the discretisation one δ_D. The first one is negligible compared to the others because of the double-precision nature of the calculations. Iterative error is related to equations resolution, so it can be minimised by reaching a convergence level close to machine accuracy. Reaching such kind of convergence can be easy once steady flow conditions are examined; however, for unsteady flow assumption, this grade of convergence is hard to reach. In any case, once the convergence level between two consecutive iterations is lower than 10^{-3}, then the iterative error can be considered of a lower level compared to the discretisation one, so the following assumption can be made:

$$\delta_{SN} = \delta_D + \delta_I \approx \delta_D \tag{B.1}$$

A possible way to determine δ_D is to perform a mesh independence study on similar meshes with different levels of resolution and evaluate

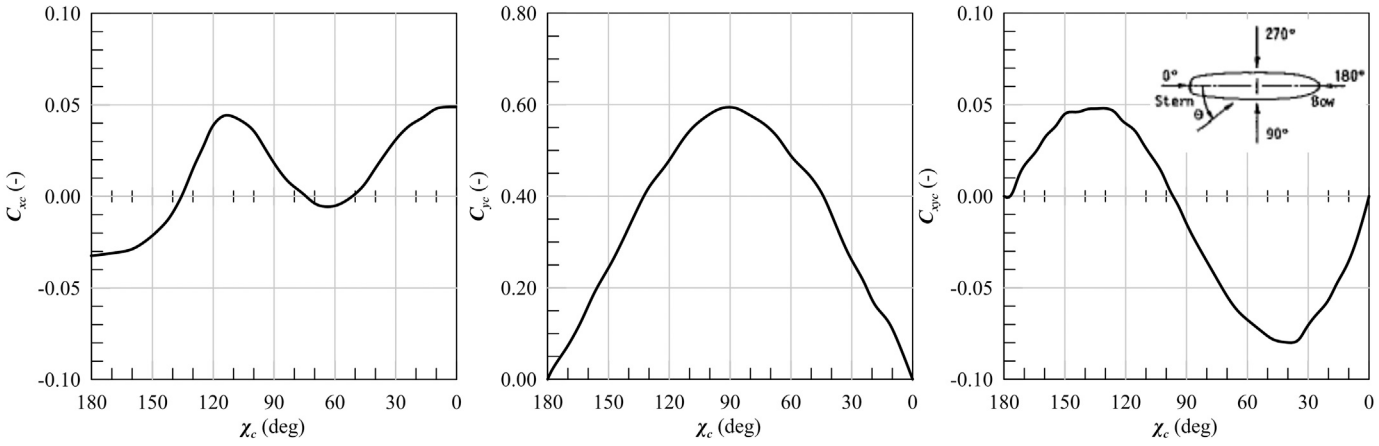

Fig. A.1. OCIMF current loads coefficients and reference system for fully loaded VLCCs.

using the Grid Convergence Index (GCI) the asymptotic region of the solution compared to the real value ϕ_0 determined through the Richardson extrapolation. To achieve the mesh-independence study, it is essential to have a calculation domain parametrised, to capture the effect of cell dimensions on the final solution. For this reason, all the refinement blocks have been parametrised as a function of the mesh base size parameter B_S. So considering a constant refinement ratio h, starting from an initial base size value B_{S_0}, a set base sizes B_{S_i} is determined. Then, it is possible to determine δ_D as follows:

$$\delta_D \approx \phi_i - \phi_0 = \epsilon_e \left(\frac{B_{S_i}}{B_{S_0}} \right)^{p_a} \tag{B.2}$$

where ϵ_e is a constant and p_a is the observed order of accuracy. The other terms are defined as follows:

$$B_{S_i} = \begin{cases} B_{S_0} h & \text{for } B_{S_i} < B_{B_{S_0}} \\ B_{S_0} / h & \text{for } B_{S_i} > B_{B_{S_0}} \end{cases} \tag{B.3}$$

The definition of Eq. (B.3) allows for considering both coarser and finer grids compared to the base one. Then the uncertainty U_D can be estimated (Eca et al., 2010) by applying a safety factor F_s to the obtained error, and, remembering equation (B.1), the uncertainty of the numerical simulation becomes:

$$U_{SN} = U_D + U_I \approx U_D \tag{B.4}$$

On the other hand, also the data coming from the experimental tests are subjected to an error δ_E and a relative uncertainty U_E. For this reason, also experimental uncertainty should be determined. However, once a detailed investigation is not possible because model tests are not performed by the same parties, then the assumptions and guidelines given by the dedicated committees for experimental test should be used. In the case of towing tank experiments, U_E has been selected equal to the 2.5% of the measured value, as the average value given by the most important hydrodynamics institutes; however, once the tests could be autonomously performed, uncertainty can be determined in a more precise way (ITTC, 2014). Then, the total uncertainty of the process U_P can be determined as:

$$U_P = \sqrt{U_{SN}^2 + U_E^2} \tag{B.5}$$

Having determined the total uncertainty of the process, it is then possible to compare the uncertainty with the comparison error δ_C. As an alternative, it is also possible to avoid the calculation of U_P and evaluate directly the total error of the process δ_P in the following form (ASME, 2009):

$$\delta_P = \delta_c - \left(\delta_{SN} - \delta_E \right) \tag{B.6}$$

However, through this study, the second option has not be applied, preferring the approach based on the uncertainty determination. To establish whether a simulation can be considered validated with the experimental data, the following criterion has been applied:

$$\begin{cases} |\delta_c| < U_P & \text{validated} \\ |\delta_c| > U_P & \text{not validated} \end{cases} \tag{B.7}$$

In fact, when U_P is much lower than δ_C, δ_{SN} is relatively high, which means that the problem modelling should be improved. On the other hand, when δ_C is lower than the total uncertainty, the problem modelling can be considered enough accurate, and the calculation can be than considered validated.

To proceed with the validation process of a grid suitable to perform current calculations on drill-ships, a suitable open-access geometry with available experimental results needs to be selected. On this purpose, the KRISO Very Large Crude Carrier 2 (KVLCC2) hull form presents a suitable test case for current calculations on large C_B vessels. The hull is representative of a 300 000 t tanker of the 1997, fitted with a bulbous stern with U-shaped sections. This vessel has been used for a lot of reference studies on ship manoeuvring, so data are available for different conditions, including cross-flow directions.

This appendix presents the results of a sensitivity study for the incidence angle $\chi_c = 15$ degrees, corresponding to $Re = 3.27 \cdot 10^6$. The mesh size and the refinements are parametrised as a function of a base size B_s, so that they can be easily modified during the sensitivity study. Here, a constant refinement ratio of 1.25 is used between adjacent grids.

Table B.1 presents the sensitivity study results, reporting the mesh dimensions and the obtained GCI. For the presented case, the convergence can be assumed in the transition between grid 2 and grid 1; therefore, grid 2 is taken as a suitable mesh for the stated numerical problem and the associated geometry. The non-dimensional values reported in Table B.1 are different from the ones considered through the study. In fact, for the present application, the following non-dimensional coefficients are adopted, to be compliant with the experimental data (Toxopeus and Lee, 2008):

$$X' = \frac{F_{X_c}}{\frac{1}{2}\rho_w L T_d V_c^2} \tag{B.8}$$

$$Y' = \frac{F_{Y_c}}{\frac{1}{2}\rho_w L T_d V_c^2} \tag{B.9}$$

$$N' = \frac{M_{Z_c}}{\frac{1}{2}\rho_w L^2 T_d V_c^2} \tag{B.10}$$

The results of the sensitivity study are presented in Fig. B.1 for all three quantities related to the forces and moments in the horizontal plane. As it can be seen, in such a case, all three quantities can be considered validated for the presented χ_c angle, since the condition given by Eq. (B.7) is satisfied for all the cases. The errors have been

Table B.1
Mesh sensitivity study on KVLCC2 geometry for $\chi_c = 15$ degrees.

Grid	Cells	B_s	X'	Y'	N'	GCI		
			–	–	–	X'	Y'	N'
1	7823672	$0.168L$	−0.0160	−0.1020	−0.0301	–	–	–
2	4467021	$0.210L$	−0.0158	−0.1013	−0.0305	0.284	0.120	0.415
3	2321892	$0.268L$	−0.0145	−0.0956	−0.0325	1.527	0.791	1.705
4	1352609	$0.328L$	−0.0135	−0.0854	−0.0341	1.939	2.349	1.868

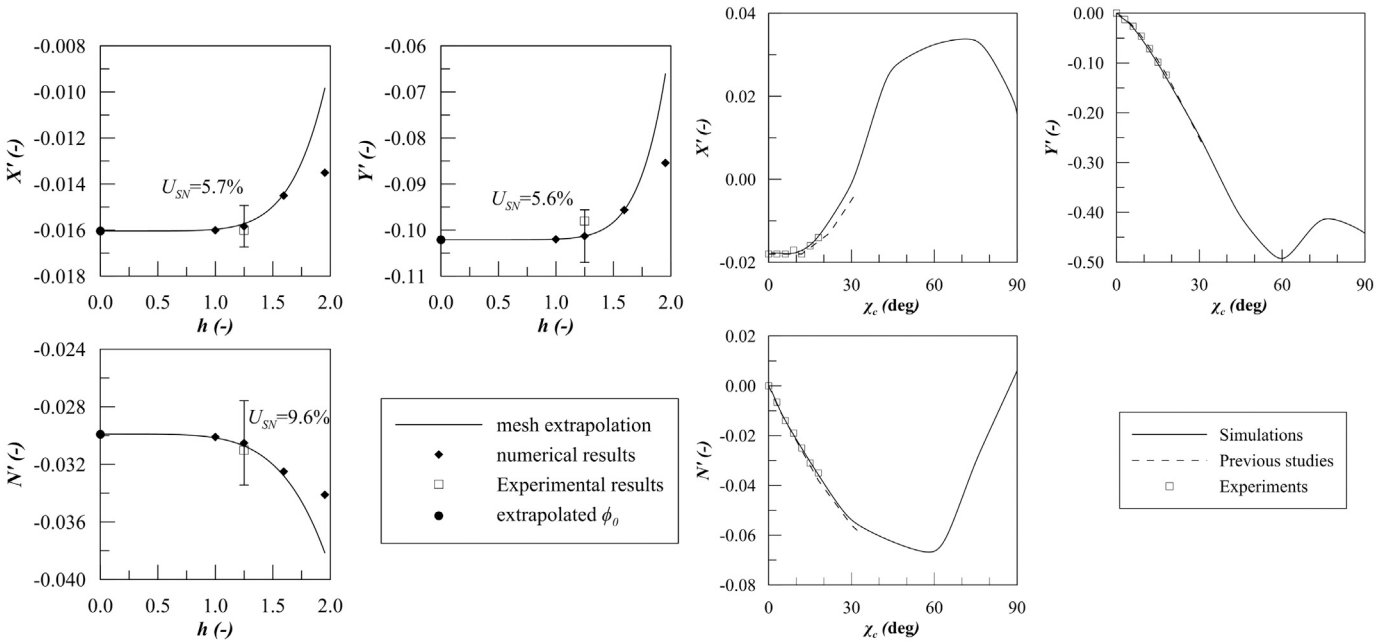

Fig. B.1. Validation study at $\chi_c = 15$ degrees (*left*) and comparison with experimental results and previous numerical studies (*right*) on the KVLCC2.

calculated according to the presented procedure; however, determining the experimental error is still a matter of uncertainty.

Compared to the studies presented in Toxopeus and Lee (2008), here the values are validated also for the lateral force, stating that the modelling can be considered satisfactory for such kind of incidence angle.

On the present geometry, calculations were carried out also at incidence angles above the standard ones tested in conventional manoeuvring benchmark tests. These cases cover a drift angle range outside the drift angles at which validation material is available in the literature. However, a previous study performed on the same geometry employing CFD calculations (Toxopeus, 2011) highlights that the calculation results are in line with the proposed one up to an angle of 30 degrees. Fig. B.1 compares the obtained coefficients, the previous study and the experimental ones. It can be observed that the obtained values are in line with the experimental data and they have a validation level higher than the curves presented in Toxopeus (2011).

However, it is advisable to increase the reliability of the proposed mesh strategy and of the numerical setup by ensuring the mesh independence also for higher heading angles, where flow separation occurs.

The sensitivity analysis is performed at the same Reynolds number of the validation at $\chi_c = 15$ degrees, selecting as reference headings $\chi_c = 60$ and $\chi_c = 90$ degrees. These two angles represent conditions with sure occurrence of flow separation. For the heading of 60 degrees, the force components X' and Y' have a significant contribution to the total loads together with moment N'. For 90 degrees the Y' component is predominant while the longitudinal force and the moment should be close to 0.

Tables B.2 and B.3 report the results of the mesh sensitivity analysis for 60 and 90 degrees, respectively. The analysis is performed employing the same refinements and base sizes B_s of the validation study at $\chi_c = 15$ degrees, resulting in four meshes having a number of cells comparable with the previous study. Analysing the results, some differences can be noticed with the mesh sensitivity at small heading angles. At small headings the transition of the observed X', Y' and N' values is monotonic with the B_s increase. At both 60 and 90 degrees this is not always true, especially for X' component. In fact the coarsest mesh (Grid 4) presents values that are in antithesis with the progression of the three other meshes. Such a behaviour is due to the presence of flow separation, that in such a case cannot be adequately captured by the coarser meshes. In any case, considering the GCI values, it can be stated that the transition between grid 2 and grid 1 lays in the asymptotic region of the convergence as for the $\chi_c = 15$ degrees. Therefore, grid 2 is a suitable refinement also for the higher incidence angles as it was for the validation study performed at 15 degrees. Even though the high incidence angle cases cannot be validated with experimental data, the sensitivity study ensures that the discretisation error remains small and consequently the uncertainty of the numerical simulation U_{SN} is comparable with the validation study at 15 degrees.

For such a reason, it is reasonable to assume that calculations made with the proposed physical modelling and meshes are sufficiently accurate for current force estimation in early-stage design.

Table B.2
Mesh sensitivity study on KVLCC2 geometry for $\chi_c = 60$ degrees.

Grid	Cells	B_s	X'	Y'	N'		GCI	
			–	–	–	X'	Y'	N'
1	7285421	$0.168L$	0.0344	−0.4968	−0.0670	–	–	–
2	4234019	$0.210L$	0.0324	−0.4928	−0.0664	1.548	0.409	1.177
3	2231892	$0.268L$	0.0214	−0.4791	−0.0653	9.190	1.422	2.317
4	1253701	$0.328L$	0.0344	−0.5082	−0.0632	16.373	3.102	4.111

Table B.3
Mesh sensitivity study on KVLCC2 geometry for $\chi_c = 90$ degrees.

Grid	Cells	B_s	X'	Y'	N'		GCI	
			–	–	–	X'	Y'	N'
1	7275397	$0.168L$	0.0178	−0.4430	−0.0063	–	–	–
2	4219123	$0.210L$	0.0159	−0.4438	−0.0059	5.247	0.005	1.296
3	2212580	$0.268L$	0.0089	−0.4827	−0.0016	21.241	0.227	12.035
4	1231897	$0.328L$	0.0109	−0.5236	−0.0015	10.952	0.220	0.620

Appendix C. Regression model

As already mentioned, the CFD results have been obtained from a set of hull forms determined with a Box-Behnken method; therefore, the surrogate model resulting from an RSM should be a second-order multiple linear regression. Once a second-order model is utilised using the response surface methodology, the regression model becomes:

$$y = \beta_{r_0} + \sum_{i=1}^{n} \beta_{r_i} x_i + \sum_{i=1}^{n-1} \sum_{j=i+1}^{n} \beta_{r_{ij}} x_i x_j + \sum_{i=1}^{n} \beta_{r_{ii}} x_i^2 + \epsilon_r, \tag{C.1}$$

where β_{r_i}, $\beta_{r_{ij}}$ are unknown parameters and ϵ_r is the random error. The unknown parameters are usually determined by using the least square method. Adopting a matrix formulation, Eq. (C.1) becomes:

$$\boldsymbol{Y} = \boldsymbol{bX} + \boldsymbol{\epsilon_r}, \tag{C.2}$$

where $\boldsymbol{Y}$ is the matrix of measured values, $\boldsymbol{X}$ is the matrix of independent variables, $\boldsymbol{b}$ is the matrix of coefficient and $\boldsymbol{\epsilon_r}$ is the matrix of errors. Using the matrix formulation, the unknown of the problem is the matrix $\boldsymbol{b}$, which is obtained as follows:

$$\boldsymbol{b} = \left(\boldsymbol{X'X}\right)^{-1} \boldsymbol{X'Y}, \tag{C.3}$$

where $\boldsymbol{X'}$ is the transpose of matrix $\boldsymbol{X}$ and $\left(\boldsymbol{X'X}\right)^{-1}$ is the inverse of $\boldsymbol{X'X}$.

C.1. Current loads regression model

As mentioned, the application of the Box-Behnken DOE implies the adoption of a second-order RSM. Therefore, the generic model of Eq. (C.1) for the current loads, considering 3 variables ($x_1 = L/B$, $x_2 = B/T_d$ and $x_3 = C_B$), becomes:

$$\begin{aligned} y \;=\; & \beta_{r_0} + \beta_{r_1} x_1 + \beta_{r_2} x_2 + \beta_{r_3} x_3 + \beta_{r_{12}} x_1 x_2 + \\ & + \beta_{r_{13}} x_1 x_3 + \beta_{r_{23}} x_2 x_3 + \beta_{r_{11}} x_1^2 + \beta_{r_{22}} x_2^2 + \beta_{r_{33}} x_3^2 \end{aligned} \tag{C.4}$$

Then, Eq. (C.4) is the basis for the development of the current surrogate model, which has the following formulation for the current form factors:

$$\begin{aligned} k_x\left(\chi_c\right) \;=\; & a_0 + a_1\left(L/B\right) + a_2\left(B/T_d\right) + a_3\left(C_B\right) + \\ & + a_4\left(L/B\right)\left(B/T_d\right) + a_5\left(L/B\right)\left(B/T_d\right) + \\ & + a_6\left(B/T_d\right)\left(C_B\right) + a_7\left(L/B\right)^2 + \\ & + a_8\left(B/T_d\right)^2 + a_9\left(C_B\right)^2 \\ k_y\left(\chi_c\right) \;=\; & b_0 + b_1\left(L/B\right) + b_2\left(B/T_d\right) + b_3\left(C_B\right) + \\ & + b_4\left(L/B\right)\left(B/T_d\right) + b_5\left(L/B\right)\left(B/T_d\right) + \\ & + b_6\left(B/T_d\right)\left(C_B\right) + b_7\left(L/B\right)^2 + \\ & + b_8\left(B/T_d\right)^2 + b_9\left(C_B\right)^2 \end{aligned} \tag{C.5}$$

$$\begin{aligned} k_{Mz}\left(\chi_c\right) \;=\; & c_0 + c_1\left(L/B\right) + c_2\left(B/T_d\right) + c_3\left(C_B\right) + \\ & + c_4\left(L/B\right)\left(B/T_d\right) + c_5\left(L/B\right)\left(B/T_d\right) + \\ & + c_6\left(B/T_d\right)\left(C_B\right) + c_7\left(L/B\right)^2 + \\ & + c_8\left(B/T_d\right)^2 + c_9\left(C_B\right)^2 \end{aligned} \tag{C.6}$$

Eqs. (C.5), (C.6) and (C.7) represent the complete general regression model for the current form factors. Regressions have been performed on 11 angles χ_c, corresponding to 0.0, 7.5, 15.0, 30.0, 60.0, 90.0, 120.0, 150.0, 165.0, 172.5 and 180.0 degrees. As the k_y and k_{Mz} coefficients are close to 0 for χ_c od 0.0 and 180 degrees, no regressions have been performed for these angles.

C.2. Drill ship wetted surface

The proposed method for the current modelling employs regressions for a non-dimensional form factor. However, for station-keeping evaluation, the dimensional forces are required, thus, the application of Eqs. (4), (5) and (6) is needed. The equations include the vessel wetted surface S; therefore, also S should be determined as a function of the main design parameters. In fact, S is not a parameter that is available in the early-stages of design, as its accurate determination needs the development of the hull geometry. Therefore, thanks to the developed systematic series of drill-ships, it is possible to estimate S with a regression model by employing the same methodology developed for the non-dimensional current load coefficients.

For the wetted surface, the following MLR formulation can be used:

$$\begin{aligned} S \;=\; & d_0 + d_1\left(L/B\right) + d_2\left(B/T_d\right) + d_3\left(C_B\right) + \\ & + d_4\left(L/B\right)\left(B/T_d\right) + d_5\left(L/B\right)\left(B/T_d\right) + \\ & + d_6\left(B/T_d\right)\left(C_B\right) + d_7\left(L/B\right)^2 + \\ & + d_8\left(B/T_d\right)^2 + d_9\left(C_B\right)^2 \end{aligned} \tag{C.8}$$

Also in this case, Eq. (C.8) is representative of the full regression model; however, Table C.1 reports the significant coefficients d_i obtained with the same step-wise process employed for the previous regressions. From the table, it results that the regression is significant to the initial population of wetted surfaces, presenting a good agreement in fitting the data. The adopted regression is significant to the developed systematic series of hull forms and is alternative to other statistical method like the one of Holtrop and Mennen (Holtrop and Mennen, 1978) for the initial estimate of S. With the regression on S all the quantities needed for the evaluation of the current loads are available, just knowing L, B, T_d and Δ.

Table C.1
Regressions coefficients and goodness of fit for S.

	d_0	d_1	d_2	d_3	d_4	d_5	d_6	d_7	d_8	d_9
	3.1010e4	2.2572e4	−5.4004e4	−2.2991e4	−2.0567e3	−1.6028e4	4.3582e4	–	4.2800e4	–
F					10.9683					
p-val					0.0027					
R^2					0.9164					
R^2_{adj}					0.8329					

References

Aalberts, A., Kuipers, R., van Walree, F., Jansen, R., 1995. Developments in dynamic positioning systems for offshore stationkeeping and offloading. In: ISOPE Conference.

API, 1984. API 2P-RP 1984. Technical Report, American Petroleum Institute.

Ardavanis, K., Nabergoj, R., Mauro, F., 2022. DP challenges in ANA platform jacket installation. Brodogradnja 73, 1–11.

Arditti, F., Cozijn, H., Van Daalen, E., Tannuri, E., 2019. Robust thrust allocation algorithm considering hydrodynamic interactions and actuator physical limitations. J. Marine Sci. Technol. (Japan) 24, 1057–1070.

Arditti, F., Souza, F., Martins, T., Tannuri, E., 2015. Thrust allocation algorithm with efficiency function dependent on the azimuth angle of actuators. Ocean Eng. 105, 206–216.

ASME, 2009. Standard for Verification and Validation in Computational Fluid Dynamics and Heat Transfer. Technical Report, American Society of Mechanical Engineers.

Aydın, Ünal, U., Sarıöz, K., 2022. Computation of environmental loads towards an accurate dynamic positioning capability analysis. Ocean Eng. 243, 110201.

Bailey, D., 1976. The Npl High Speed Round Bilge Displacement Hull Series. In: RINA Maritime Technology Monograph, vol. 4.

Box, G., Behnken, D., 1960. Technometrics. Wiley, New York.

Box, G., Hunter, W., Hunter, J., 1978. Statistics for Experiments. Wiley, New York.

Chang, H., 2008. A data mining approach to dynamic multiple responses in Taguchi experimental design. Expert Syst. Appl. 35, 1095–1103.

Della Loggia, B., Doria, L., 1980. Methodical series tests for fuller ship hull forms. Ocean Eng. 7, 659–706.

DNV-GL, 2018. DNVGL-ST-0111: Assessment of Station Keeping Capability of Dynamic Positioning Vessels. Technical Report, DNV-GL.

Eca, L., Vaz, G., Hoekstra, M., 2010. Code verification, solution verification and validation in RANS solvers. In: 29th International Conference on Ocean, Offshore and Artic Engineering OMAE. Shangahai, China.

Ferrari, V., Kisjes, A., Quadvlieg, F., 2019. Influence of skeg on ship manoeuvrability at high and low speeds. In: Proceedings of the 14th International Symposium on Practical Design of Ships and Other Floating Structures PRADS 2019.

Ferziger, J., Perić, M., 2002. Computational Methods for Fluid Dynamics, third rev. ed. Springer-Verlag, Berlin.

Holtrop, J., Mennen, G., 1978. A Statistical Power Prediction Method. Int. Shipbuild. Prog. 25.

IMCA, 2000. Specification for DP Capability Plots IMCA M 140 Rev. I. Technical Report, The International Marine Contractors Association.

ITTC, 2011. Recommended Procedures and Guidelines: Practical Guidelines for Ship CFD Applications ITTC 7.5-03-02-03. Technical Report, International Towing Tank Conference.

ITTC, 2014. Recommended Procedures and Guidelines; Example for Uncertainty Analysis of Resistance Test in Towing Tank. ITTC 7.5-02-02-01. Technical Report, International Towing Tank Conference.

Kim, J., Hong, C., Lee, D., Ahn, S., 2009. Prediction of current load using computational fluid dynamics. In: Proceedings of the International Conference on Offshore Mechanics and Arctic Engineering. OMAE, pp. 359–366.

Koop, A., 2015. Shallow water current loads on a lng carrier using cfd. In: Proceedings of International Conference on Ocean, Offshore and Artic Engineering. St. John's, Canada.

Koop, A., 2020. Using cfd to determine scale effects on current loads of offshore vessels in side-by-side configuration. Ocean Eng. 195, 106707.

Koop, A., Klaij, C., G.V, 2013. Viscous-flow calculations for model and full-scale current loads on typical offshore structures. Comput. Methods Appl. Sci. 29, 3–29.

Martelli, M., Faggioni, N., Donnarumma, S., 2022. A time-domain methodology to assess the dynamic positioning performances. Ocean Eng. 247, 110668.

Mauro, F., 2019. Enhanced Station Keeping Analysis in Early Design Stage of Offshore Vessels (Ph.D. thesis). University of Rijeka.

Mauro, F., Benci, A., Ferrari, V., Della Valentina, E., 2020. Dynamic positioning analysis for the early-design stage of large yachts. In: Proceedings of the 26th HISWA Symposium on Yacht Design and Constructions.

Mauro, F., Benci, A., Ferrari, V., Della Valentina, E., 2021. Dynamic positioning analysis and comfort assessment for the early design stage of large yachts. Int. Shipbuild. Progr. 68, 33–60.

Mauro, F., Duranti, E., 2018. Effect of propeller modelling on station-keeping thruster allocation strategy. In: Technology and Science for the Ships of the Future - Proceedings of NAV 2018: 19th International Conference on Ship and Maritime Research. pp. 356–363.

Mauro, F., Gaudiano, F., 2018. Station-keeping calculations in early design stage: two possible approaches. In: NAV 2018 Conference. Triest, Italy.

Mauro, F., Nabergoj, R., 2015. Smart thrust allocation procedures in early design stage dynamic positioning predictions. In: 18th International Conference on Ships and Shipping Research, NAV 2015. pp. 1011–1019.

Mauro, F., Nabergoj, R., 2016. Advantages and disadvantages of thruster allocation procedures in preliminary dynamic positioning predictions. Ocean Eng. 123, 96–102.

Mauro, F., Nabergoj, R., 2019. Optimal thruster location on offshore DP vessels. Int. Shipbuild. Prog. 66, 145–162.

Mauro, F., Nabergoj, R., 2022. A probabilistic approach for dynamic positioning capability and operability predictions. Ocean Eng. 262, 112250.

Mauro, F., Prpić-Oršić, J., 2020. Determination of a dp operability index for an offshore vessel in early design stage. Ocean Eng. 195, 106764.

Nabergoj, R., 2011. Station-keeping and seakeeping in offshore vessel design. In: Proceedings of 1st INT-NAM 2011. Istanbul, Turkey.

OCIMF, 1994. Prediction of Wind and Current Loads on VLCCs, Second Edition. Technical Report, OCIMF.

OCIMF, 2010. Estimating the Environmental Loads on Anchoring Systems. Technical Report, Oil Companies International Marine Forum OCIMF.

Ottens, H., Van Dijk, R., Meskers, G., 2009. Benchmark study between cfd and model tests on a semi-submersible crane vessel. In: Proceedings of the International Conference on Offshore Mechanics and Arctic Engineering - OMAE. pp. 671–682.

Patankar, S., 1980. Numerical Heat Transfer and Fluid Flow. McGraw-Hill, New York.

Rhie, C., Chow, W., 1983. A numerical study on turbulent flow past an isolated airfoil with trailing edge separation. AIAA J. 21, 1525–1532.

Roache, P., 1998. Verification and Validation in Computational Science and Engineering. Hermosa Publisher, Albuquerque.

Roseman, D., 1987. The MARAD systematic series of full-form ship models. In: The Society of Naval Architects and Marine Engineers. SNAME, Jersy City, NJ, USA.

Smogeli, O., Trong, N., Borhaug, B., Pivano, L., 2013. The next level DP capability analysis. In: Dynamic Positioning Conference.

STARCCM, https://plm.sw.siemens.com/en-us/simcenter/fluids-thermal-simulation/star-ccm.

Swift, P., Nowacki, H., Fischer, J., 1973. Estimation of great lakes bulk carrier resistance based on model test data regressions. In: Marine Technology.

Todd, F., 1963. Series 60 Methodical Experiments with Models of Single-Screw Merchant Ships. Technical Report, David Taylor Model Basin, Washington DC, USA.

Toxopeus, S., 2011. Practical Application of Viscous-Flow Calculations for the Simulation of Maneouvring Ships (Ph.D. thesis). Delft University of Technology.

Toxopeus, S., Lee, W., 2008. Comparison of manoeuvring simulation programs for SIMAN test cases. In: SIMMSN Workshop on Verification and Validation of Ship Manoeuvring Simulation Methods. Copenhagen, Denmark.

Vaz, G., Waals, O., Ottens, H., Fathi, F., Le Souëf, T., Kiu, K., 2009. Current affairs: Model tests, semi-empirical predictions and cfd computations for current coefficients of semi-submersibles. In: Proceedings of the International Conference on Offshore Mechanics and Arctic Engineering - OMAE. pp. 877–887.

Vroegrijk, E., 2017. OCIMF CFD Current Drag 1610-0043-Revision 2. Technical Report, Lloyd Register.

Wang, I., Yang, J., Xu, S., 2018. Dynamic positioning capability analysis for marine vessels based on DPCAP polar diagram. China Ocean Eng. 32, 90–98.

Wilcox, D., 1998. Turbulence Modelling for CFD, second ed. DCW Industries Inc.

Yuck, R., Hong, S., Choi, H., 2005. Estimation of current loads on offshore vessels. In: Proceedings of the International Offshore and Polar Engineering Conference.